UNIMORE
UNIVERSITÀ DEGLI STUDI DI
MODENA E REGGIO EMILIA

Dipartimento di Scienze Chimiche e Geologiche

Corso di Laurea Magistrale in Geoscienze, Georischi e Georisorse

Assessing Landslide Susceptibility and Changes in Human Exposure in the Lisbon Region (Portugal)

Relatore:

Prof. Mauro Soldati

Laureando:

Marco Paganelli

Correlatori:

Prof. Jose Luis Gonçalves Moreira Da Zezere

Prof.ssa Raquel Susana Dos Reis Alcântara Melo

Dr. Alessandro Ghinoi

Anno accademico 2024/2025

ABSTRACT

Landslides represent one of the most significant geomorphological hazards worldwide, generating substantial economic losses and social impacts, particularly in rapidly urbanising regions. In Portugal, the Lisbon region has experienced continuous urban expansion over recent decades, leading to an increasing concentration of buildings, infrastructure and population in potentially unstable slopes. In this context, understanding landslide susceptibility and how exposure has evolved in this region is essential for supporting land-use planning and risk mitigation strategies.

This study assesses landslide susceptibility and quantifies population exposure at the municipal scale in the Lisbon region, considering a study area of about 3,006 km^2.

The landslide susceptibility modelling was performed using the Information Value (IV) method, a bivariate statistical approach that quantifies the relationship between landslide occurrence and landslide predisposing factors. A landslide inventory updated up to 2021, comprising 4,018 landslide polygons, was used as the dependent variable. The inventory was randomly divided into three subsets for three-fold cross-validation. Eight independent variables were considered, and their values were grouped into classes: slope angle, elevation, aspect, plan curvature, Topographic Wetness Index (TWI), Topographic Position Index (TPI), geology and soil type. The topographic parameters were derived from a 10 m resolution Digital Elevation Model (DEM), while lithological and soil data were obtained from official thematic maps. Model predictive performance was evaluated through prediction-rate curves and the Area Under the Curve (AUC) on the validation subsets, showing a value of about 0.90, signifying that 90% of the total landslide covered area is concentrated only in 16.75% of the study area, providing an independent assessment of robustness and potential overfitting. The final Landslide Susceptibility Map was produced by averaging the IV-based susceptibility scores obtained across the three cross-validation folds and defining susceptibility thresholds based on the cumulative distribution of landslide area.

To quantify exposure, the susceptibility map was intersected with census-based buildings and resident population datasets, as well as road network data, for 2021, and compared with equivalent 2011 datasets. This multitemporal approach enables the quantification of changes in

exposure between 2011 and 2021, a decade marked by continued urban growth in several municipalities. Results highlight significant spatial heterogeneity in exposure patterns, with densely urbanised municipalities such as Lisboa, Sintra, Cascais and Loures concentrating a substantial proportion of buildings and resident population within high and very high landslide susceptibility classes. Between 2011 and 2021, the expansion of built-up areas in selected municipalities suggests a progressive increase in exposure where urban development overlaps these susceptibility classes, potentially increasing landslide risk.

Although susceptibility does not directly quantify temporal probability or physical vulnerability, the integration of statistically validated susceptibility models with detailed exposure data provides a consistent and reproducible framework for municipal-scale risk-informed planning. The results provide a scientific basis for territorial planning, infrastructure management and civil protection strategies aimed at reducing future socio-economic losses associated with slope instability.

SUMMARY

INTRODUCTION

Landslides are defined as the movement of rock, debris or earth down a slope [1]. They often occur along pre-existing discontinuities or failure surfaces when driving forces exceed resisting forces, causing the mobilized material to move downslope and eventually deposit when the slope angle decreases and the material loses velocity.

A landslide can be described by both the type of material involved and the type of movement. Landslide movements are classified into falls, flows, slides, spreads and topples, as well as complex (or composite) landslides, which involve a combination of two or more of these movement types [1].

Despite improved understanding of slope instability mechanisms and the availability of a wide range of mitigation techniques, landslides continue to be responsible for significant economic losses and casualties worldwide [2]. Landslide risk represents the potential losses resulting from the occurrence of slope instability processes and is generally defined as the product of hazard, vulnerability and the value of the exposed elements [3]. Quantitative Risk Analysis (QRA) allows these components to be integrated in an objective and reproducible manner. It enables comparison between different spatial units, evaluation of magnitude scenarios and support for cost–benefit analysis of mitigation measures. At the municipal scale, risk analysis provides essential information for land-use planning, civil protection and infrastructure management, particularly in rapidly urbanizing regions.

Landslide hazard refers to the probability of occurrence of landslides of a given magnitude within a defined area and time period [4]. In many regional-scale studies, the temporal recurrence of landslide events (i.e., the frequency or return period of occurrence within a defined time window) is poorly constrained due to incomplete event dating and short or non-systematic records. As a result, a fully quantitative hazard assessment that combines spatial and temporal probabilities is often not feasible, and landslide susceptibility is used to represent the spatial component of hazard. Landslide susceptibility indicates where landslides are more likely to occur and can be assessed at the regional scale, even when detailed information on landslide typology is not fully available, by comparing the landslide distribution with a set of assumed independent landslide predisposing factors [1].

Vulnerability to landslides is widely recognized as a multidimensional concept that describes the degree of loss expected for elements exposed to a landslide event [3].

The assessment of vulnerability involves in many cases the evaluation of several different parameters and factors, such as building materials and techniques, the state of conservation, the presence of protection structures and the presence of warning systems [5,6].

In landslide risk analysis, vulnerability is generally divided into two main components: social vulnerability and physical vulnerability. Physical vulnerability refers to the expected degree of structural damage affecting buildings and infrastructure when impacted by a landslide of a given magnitude. It is defined as a functional relationship between process magnitude and expected damage and is commonly expressed on a scale ranging from 0 (no loss) to 1 (total loss) [3]. Physical vulnerability depends on building typology, construction materials, structural resistance and landslide characteristics such as depth, velocity and volume.

The vulnerability of people depends on many factors, such as the landslide type, size and intensity; the resistance and mobility of the individuals affected by the landslide hazard; and their relative positions in the exposed area. The resistance of a person to landslides is believed to also be a function of the person's intellectual maturity (e.g. perception of the risk) and physical ability (e.g. age) [7].

The combination of social and physical vulnerability provides a more comprehensive understanding of potential impacts, as structural damage does not necessarily correspond to equal social consequences. A moderately damaged building may generate severe social disruption if it houses vulnerable populations, while structurally resistant buildings may reduce overall risk even in high-susceptibility areas. As with the temporal component of landslide hazard, many regional-scale studies do not explicitly quantify physical and social vulnerability; instead, analyses commonly focus on quantifying the exposure of elements at risk within landslide-susceptible areas.

Elements at risk refer to the population, buildings, infrastructure and economic assets that may be affected by landslides. Exposure describes the spatial distribution and concentration of these elements within areas characterized by landslide susceptibility. In municipal-scale landslide studies, the most relevant exposed elements typically include resident population, residential and non-residential buildings, transportation networks (roads, railways), and public facilities

and critical infrastructure. Exposure assessment requires detailed spatial datasets, such as census-based demographic data and building inventories. In quantitative frameworks, the economic value of buildings is often incorporated in order to estimate potential direct losses [3]. The integration of exposure data with landslide susceptibility maps (LSMs) allows the identification of areas where the concentration of people and assets overlaps with landslide-prone terrain. In LSMs, each terrain unit is associated with a numerical index that represents the spatial probability of a landslide occurrence, but LSMs do not explicitly convey information about landslide return periods [8].

It is important to emphasize that high susceptibility does not automatically imply high risk. Risk emerges when susceptible areas coincide with significant exposure and vulnerable elements. Conversely, areas with limited exposure may present low risk even if susceptibility is high. Therefore, understanding the spatial distribution and temporal evolution of exposed elements is fundamental for analysing how landslide risk may increase over time, particularly in regions undergoing rapid urban expansion.

In recent decades, parts of the Lisbon region have undergone substantial urban expansion, with consequent changes in the spatial distribution of buildings, infrastructure and population. This trend is largely driven by migration dynamics, including immigration, even though Portugal's total population is projected to decline from 10.7 million to about 8 million by 2060 [9]. Therefore, the expansion of the urban landscape in this region is likely to increase exposure where recent urban growth overlaps landslide-susceptible areas. Accordingly, the aim of this dissertation is to develop a landslide susceptibility model for the Lisbon region (Portugal) and to quantify, at the municipal scale, the exposure of buildings, resident population and road infrastructure within the highest susceptibility classes. By integrating susceptibility and exposure, the study provides a basis for identifying priority areas for risk-informed territorial planning.

CHAPTER 1: STUDY AREA

1.1. GEOGRAPHICAL SETTING AND ADMINISTRATIVE DIVISIONS

The study area (Figure 1) is located in west-central Portugal and includes most of the Lisbon district, a portion of the Santarém district and the northern part of the Setúbal district, covering an area of 3,006{Citation} km^2.

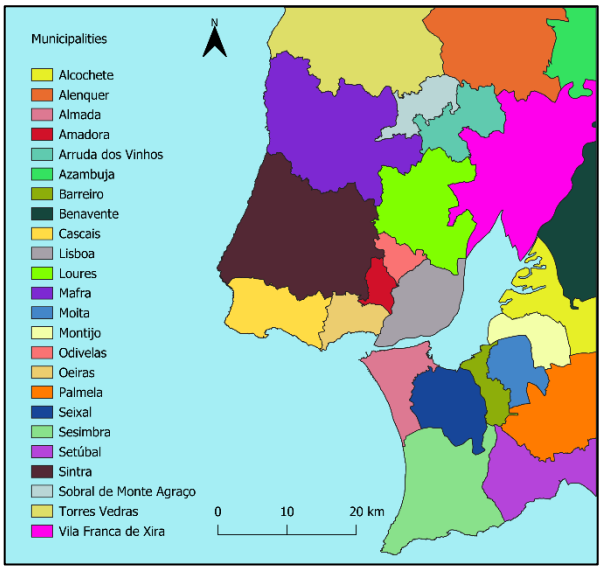

Figure 1: Subdivision of the study area at the municipal scale.

The western boundary faces the Atlantic Ocean, while the remaining boundaries are defined by adjacent municipalities and by the Tagus Estuary (Mar da Palha), associated with the Tagus River (Rio Tejo), the main river system in the area.

The study area comprises 24 municipalities, which are distributed among the three districts mentioned above: Alenquer, Amadora, Arruda dos Vinhos, Azambuja, Cascais, Lisboa, Loures, Mafra, Odivelas, Oeiras, Sintra, Sobral de Monte Agraço, Torres Vedras and Vila Franca de Xira (Lisbon district), Benavente (Santarém district), Alcochete, Almada, Barreiro, Moita, Montijo, Palmela, Seixal, Sesimbra and Setúbal (Setúbal district) (Figure 1).

These municipalities were used as the spatial reporting units for the multitemporal analysis of the exposed elements between 2011 and 2021.

1.2. GEOLOGICAL SETTING

The Lisbon region is located approximately 250 km from the Eurasia–Africa plate boundary, within a geologically complex sector of the western Iberian margin shaped by long-term tectonic, sedimentary and volcanic processes. From a morpho structural point of view, the study area is mainly included within two major geological domains: the Lower Tagus Cenozoic Basin and the Lusitanian Basin, whose interaction controls the regional geological framework and stratigraphic architecture [2,10].

The geological substratum of the Lisbon region is predominantly composed of sedimentary rocks with ages ranging from Jurassic to Pliocene, locally intruded by igneous bodies of Cretaceous age [3].

These lithologies are arranged in a complex lithostratigraphic framework characterised by strong lateral and vertical heterogeneities, reflecting the progressive infilling of sedimentary basins and subsequent tectonic deformation (Figure 2).

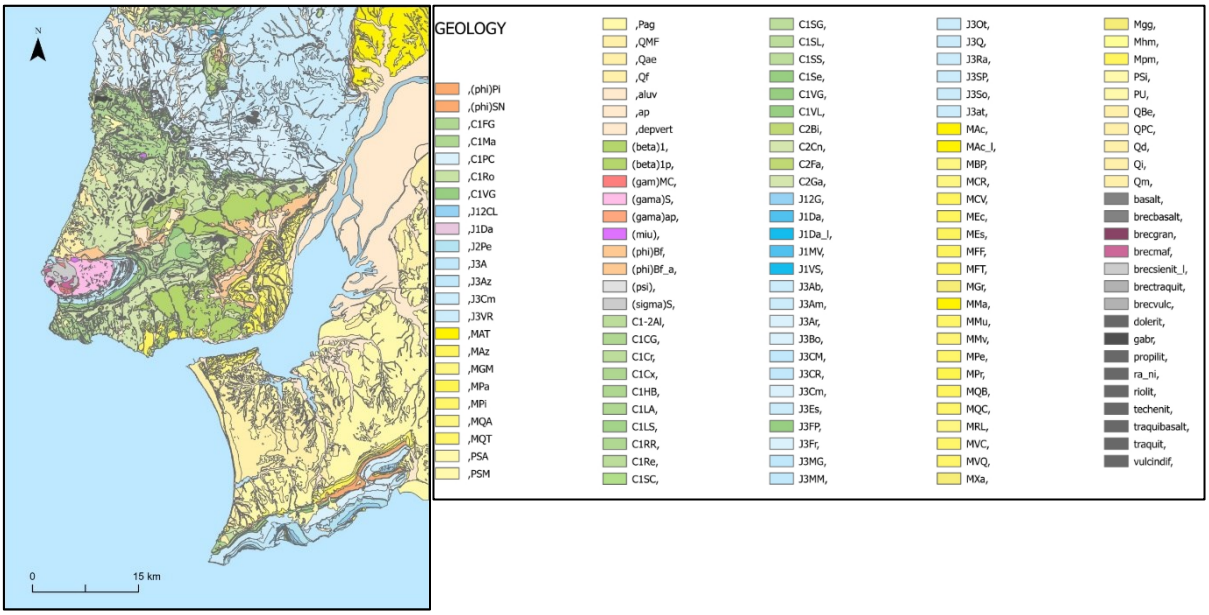

Figure 2: Geological map of the study area (left); legend of the geological map, with the codes for each lithology (right). The corresponding lithologies for each code are provided in Annex 5 in the Annex section.

The oldest units cropping out in the study area belong to the Mesozoic succession of the Lusitanian Basin and are mainly represented by Jurassic and Cretaceous formations. Jurassic units consist predominantly of carbonate and mixed carbonate–siliciclastic sequences, including limestones, marls and sandstones, which locally form the structural backbone of elevated areas. These formations are often affected by folding, faulting and intense fracturing, resulting from the long tectonic evolution of the basin and later reactivation phases [3], with structural discontinuities and differential weathering processes locally conditioning slope morphology and stability.

Cretaceous formations are widely exposed in the western and southwestern sectors of the study area and are mainly composed of limestones and marls, locally associated with volcanic rocks belonging to the Lisbon Volcanic Complex [11].

The volcanic units include basalts, breccias and volcano-sedimentary deposits, which locally form resistant lithologies but are often highly fractured. Together, the Cretaceous carbonate formations and the volcanic rocks define the geological substratum in large portions of the coastal and southwestern areas.

Cenozoic deposits related to the evolution of the Lower Tagus Basin represent a major component of the geological framework of the Lisbon region and dominate the central and eastern sectors of the study area. Paleogene formations, particularly the Benfica Formation, constitute a transitional unit between the Mesozoic substratum and younger basin infill deposits. These formations are characterised by a heterogeneous lithological composition, including conglomerates, sandstones, siltstones, claystones and marls, with marked lateral and vertical variability [2,10].

The variable grain size and frequent alternation of competent and weak layers strongly influence their mechanical behaviour.

Miocene units are among the most widespread formations in the study area and consist mainly of alternating sands, sandstones, clays, siltstones and limestones deposited in estuarine and shallow marine environments. During the Miocene, the establishment of an open connection with the sea favoured the deposition of a thick sedimentary sequence with alternating marine and continental facies [11].

These deposits form a gently east-dipping monocline, with thicknesses locally reaching approximately 300 m and progressively increasing towards the interior of the basin. Due to the frequent presence of fine-grained layers and stratigraphic contrasts, Miocene units are widely associated with slope instability processes in the region.

The youngest geological units correspond to Quaternary deposits associated with the Tagus River and its tributary network. These include Pleistocene fluvial terrace sediments and Holocene alluvial deposits composed mainly of sands, silts, clays and gravels [10].

These deposits are generally unconsolidated, highly heterogeneous and locally reach significant thicknesses in valley bottoms and low-lying areas, where they often exhibit low mechanical strength and high sensitivity to variations in water content.

Overall, the geological framework of the Lisbon region is characterised by the coexistence of competent Mesozoic bedrock, heterogeneous Cenozoic basin deposits and unconsolidated Quaternary sediments. This lithological diversity, combined with tectonic structures, stratigraphic contrasts and weathering processes, creates favourable conditions for slope instability. The geological setting therefore represents a fundamental predisposing factor for landslide occurrence and justifies the inclusion of geological units as a key predisposing factor in landslide susceptibility modelling within the study area.

1.3. GEOMORPHOLOGICAL SETTING

The geomorphological setting of the Lisbon region reflects the combined influence of tectonic structures, lithological contrasts, long-term erosion processes and fluvial dynamics associated with the Tagus River system.

The present-day landscape results from the interaction between the geological framework of the Lusitanian and Lower Tagus basins and the progressive incision and sedimentation processes that have shaped the region since the Cenozoic.

From a regional perspective, the study area is characterised by a moderately dissected relief, with elevation values ranging from sea level along the Atlantic coast and the Tagus estuary to 483 m inland [11].

This configuration results in a landscape composed of elevated interfluves separated by narrow valleys, which represent preferential pathways for surface runoff and sediment transport.

The most prominent geomorphological element of the region is the Tagus estuary (*Mar da Palha*), located in the central sector of the study area. The estuary constitutes the largest estuarine system in the Iberian Peninsula and represents a major base level for fluvial processes in the region [10].

The presence of this wide estuarine plain has favoured the development of extensive low-lying areas characterised by alluvial and estuarine deposits, particularly along the margins of the Tagus River and its tributaries.

Inland from the estuarine domain, the relief progressively increases and becomes more irregular, reflecting the structural control imposed by regional tectonics and lithological variability [11].

These factors have produced asymmetric slopes, locally steep escarpments and a heterogeneous distribution of slope gradients.

Valley morphology is strongly influenced by the geological substrate and by the history of fluvial incision. Many of the present valleys correspond to relict drainage systems that were subsequently infilled by Quaternary sediments. These valleys are often characterised by gentle to moderate slopes in their lower sections and steeper side slopes where incision into more resistant lithologies has occurred. The accumulation of fine-grained alluvial materials within valley bottoms contributes to locally high soil moisture conditions, which are particularly relevant for slope instability processes.

Coastal geomorphology also plays an important role in the western sector of the study area. The Atlantic coastline is characterised by a combination of rocky cliffs and low-lying coastal plains, where marine erosion processes interact with gravitational slope dynamics. Although coastal cliff processes are not the primary focus of this study, the presence of steep coastal slopes locally contributes to landslide susceptibility, especially where weak lithologies or structural discontinuities are present.

Overall, the geomorphological setting of the Lisbon region is marked by pronounced spatial variability in elevation, slope gradients and landform types. The alternation between hills, dissected plateaus, incised valleys and alluvial plains creates a complex topographic framework

that strongly conditions landslide occurrence. In particular, the presence of steep slopes, valley-side scarps and areas of concentrated surface runoff represents a key controlling factor for landslide susceptibility.

1.4. LANDSLIDE ACTIVITY

The geological and geomorphological framework described above provides favourable conditions for slope instability throughout the Lisbon region. The interaction between heterogeneous sedimentary formations, structural discontinuities, steep valley sides and concentrated surface runoff has historically resulted in recurrent landslide activity. Previous studies carried out in the area north of Lisbon have demonstrated that landslide occurrence is strongly influenced by a combination of predisposing factors (including lithology, slope gradient, structural setting) and rainfall-related triggering mechanisms [12].

In the region, many landslide events are associated with long-lasting or cumulative winter rainfall, which promotes progressive soil saturation, increases pore-water pressure and reduces shear strength along potential failure surfaces. However, some failures may also be triggered by short-duration, high-intensity rainfall events [12–14].

Both shallow translational slides and deep-seated rotational movements have been documented in the Lisbon region [13]. Shallow landslides are generally associated with short duration but intense rainfall, whereas deep-seated failures tend to be related to prolonged rainfall periods and progressive slope weakening [13]. This distinction reflects the influence of lithological contrasts and slope morphology, particularly in areas underlain by alternating permeable and impermeable sedimentary formations.

Spatially, landslides are preferentially distributed along steep valley sides and structural scarps, where lithological contrasts and tectonic discontinuities favour instability [12]. In addition, anthropogenic slope modifications, including road cuts and urban expansion, have been recognised as locally contributing factors to slope reactivation in the region [15], [16] .

CHAPTER 2: DATA AND MATERIALS

The reliability of landslide susceptibility and exposure assessments strongly depends on the quality, spatial resolution and consistency of the input datasets. This section describes the spatial and statistical data used in the present study, including the landslide inventory, topographic information derived from a Digital Elevation Model (DEM), official geological and soil datasets, and exposure-related datasets on buildings, resident population and road networks.

The datasets were collected from official sources and processed within a Geographic Information System (GIS) environment to ensure spatial consistency and compatibility. Both raster and vector data were harmonised to a common coordinate reference system and aligned to a 10 m × 10 m spatial resolution, corresponding to the resolution of the DEM used in this study.

The following subsections detail the characteristics, source, format and preprocessing procedures of each dataset, distinguishing between the dependent variable (landslide inventory) and the independent predisposing factors.

The selection of the predisposing factors used in landslide susceptibility assessment depends on the type of landslides, the scale of analysis and the availability of spatial data [17]. Predisposing factors represent spatial variables that influence slope stability and are assumed to control the occurrence of future landslides.

Their selection must be consistent with the dominant failure mechanisms within the study area and with the spatial resolution of the analysis [17].

Susceptibility assessment requires the identification of predisposing factors that explain the spatial distribution of past landslides, which are then used to predict the spatial probability of future occurrences [18].

In this study, eight predisposing factors were selected based on their relevance in regional-scale statistical susceptibility modelling and on data availability: six DEM-derived topographic variables and two thematic variables derived from official maps (geology and soil type).

2.1. LANDSLIDE INVENTORY

The landslide inventory (Figure 3) used in this study was updated up to 2021 and consists of 4,018 mapped landslide polygons distributed across the study area. The inventory was provided in vector format and includes geometric information (area and perimeter) for each mapped landslide.

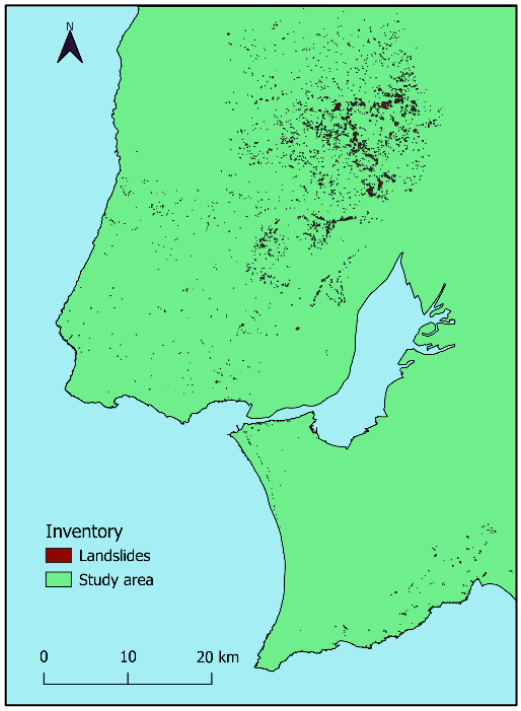

Figure 3: Complete landslide inventory (2021) for the Lisbon region.

The mapped landslide areas range from 98 m² to 273,758 m², with a mean area of 3,244 m² and a median value of 828 m². Although the dataset does not differentiate landslides by typology, the wide range of mapped areas suggests the coexistence of both shallow and deep-seated slope failures.

Shallow translational slides are the most frequent landslides in the Lisbon region and are typically small, with planar slip surfaces usually up to 1.5 m deep. They commonly occur on steep valley slopes where colluvium overlies impermeable materials such as volcanic tuffs, marls and clays. In contrast, deep-seated rotational slides are less frequent but substantially

larger, with typical slip surface depths of around 5 m, and are more commonly associated with areas where Jurassic clays and marls crop out.

For susceptibility modelling purposes, the landslide inventory was used as the dependent variable in the bivariate statistical analysis. The inventory was randomly divided into three subsets for three-fold cross-validation, allowing the generation and validation of susceptibility models using independent data in each iteration. The landslide polygons were rasterised according to the 10 m × 10 m resolution of the DEM, ensuring consistency between dependent and independent variables.

Overall, the high number of inventoried landslides confirms that the Lisbon region represents an active geomorphological system, where slope instability is a recurrent process rather than an isolated phenomenon.

This pattern is consistent with the magnitude–frequency relationships described for the area north of Lisbon, where small events occur more frequently but large landslides, although less common, are responsible for a significant proportion of direct and indirect losses [19], [15].

The availability of a large and spatially detailed inventory enhances the statistical robustness of the susceptibility modelling process. However, the absence of typological classification may limit the discrimination between different landslide mechanisms.

2.2. DIGITAL ELEVATION MODEL (DEM)

The Digital Elevation Model (DEM) used in this study corresponds to the regional *Lisboa e Vale do Tejo* (LVT) dataset and was provided in GeoTIFF format with a spatial resolution of 10 m × 10 m. The raster is stored as a 32-bit floating point dataset (Float32) and is referenced to the ETRS89 / PT-TM06 coordinate system (EPSG:3763). Elevation values are expressed in metres above sea level.

The DEM covers the entire study area with dimensions of 5485 × 7926 pixels. Elevation values range from 0 m to approximately 483 m, with a mean elevation of about 96 m. The 10 m spatial resolution ensures an adequate representation of terrain morphology at the regional scale while maintaining computational efficiency for statistical modelling.

The DEM represents the primary topographic dataset used in this study and served as the basis for the derivation of morphometric predisposing factors, including slope angle, aspect, plan curvature, Topographic Wetness Index (TWI), Topographic Position Index (TPI) and elevation. All raster-based variables were aligned to the same grid resolution and coordinate reference system to ensure spatial consistency throughout the susceptibility modelling process.

2.3. PREDISPOSING FACTORS

2.3.1. SLOPE

Slope angle is widely recognized as one of the most influential predisposing factors in landslide susceptibility modelling [17]. It directly controls the balance between gravitational driving forces and resisting forces acting along potential failure surfaces, and therefore strongly influences slope instability processes.

Commonly, it is used in heuristic, statistical and deterministic approaches to landslide susceptibility and hazard assessment and it is a key explanatory variable in regional susceptibility models, particularly for shallow landslides and translational failures [18], [17].

Slope angle was derived from the 10 m resolution DEM using the Slope tool in ArcGIS Pro (Spatial Analyst extension). The output raster was calculated in degrees (°), representing the maximum rate of elevation change between each cell and its neighbouring cells.

The resulting slope values were classified into ten classes with 5° intervals (0–5°, 5–10°, 10–15°, 15–20°, 20–25°, 25–30°, 30–35°, 35–40°, 40–45° and >45°) as shown in Figure 4, allowing the evaluation of the relationship between slope steepness and landslide occurrence within the bivariate statistical framework.

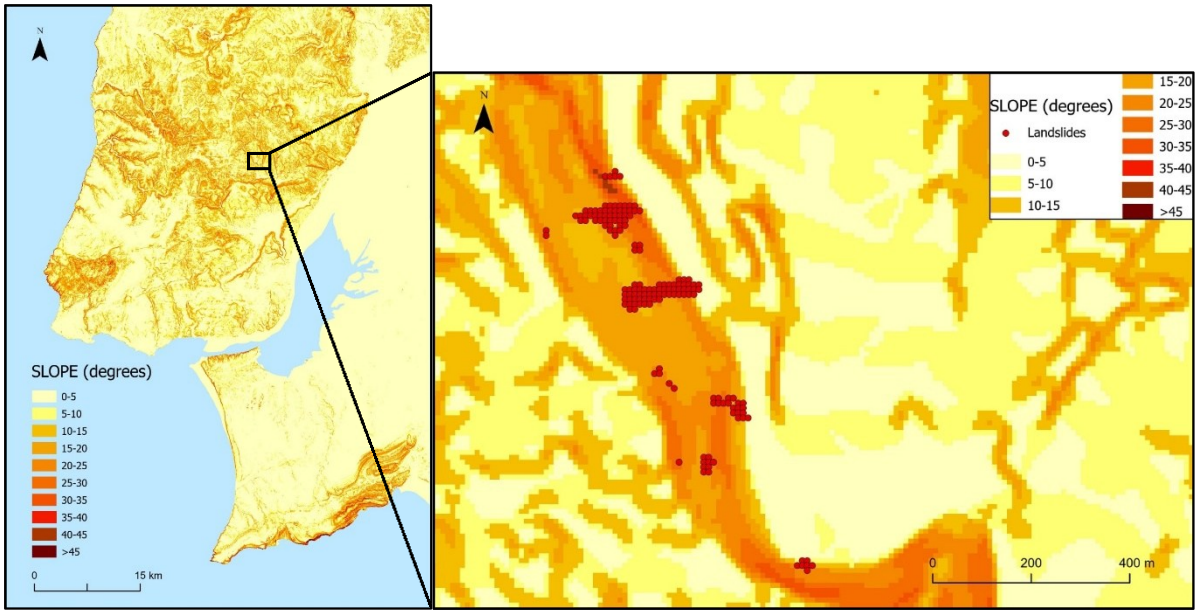

Figure 4: Slope angle map, classified into 5° intervals (left); detail of the map showing the overlap between the slope angle classes and the landslides of the inventory (right).

At the regional scale adopted in this study, the 10 m spatial resolution represents a suitable compromise between morphological detail and model stability, as the use of excessively fine-resolution DEMs may introduce local variability that does not correspond to the scale of the predisposing factors [17].

2.3.2. ELEVATION

Elevation was derived directly from the 10 m resolution DEM and represents the absolute elevation above sea level across the study area. Elevation values range from 0 m to approximately 483 m, with a mean elevation of about 96 m. The spatial distribution of elevation is shown in Figure 5, where altitudinal classes were defined at 50 m intervals (0–50 m, 50–100 m, 100–150 m, 150–200 m, 200–250 m, 250–300 m, 300–350 m, 350–400 m, 400–450 m, 450–500 m).

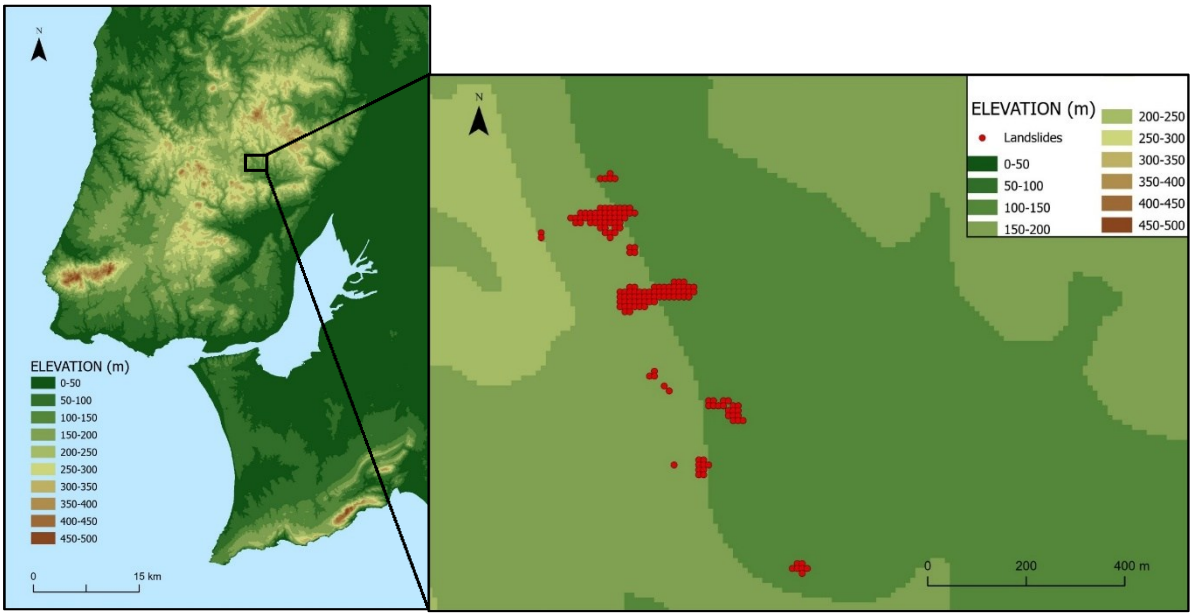

Figure 5: Elevation map of the study area, classified with 50 m intervals (left); detail of the map showing the overlap between the elevation classes and the landslides of the inventory (right).

Although elevation is not a direct mechanical control on slope failure, it is widely used in landslide susceptibility modelling as a proxy variable representing the combined effects of geomorphological, climatic and lithological conditions [17]. Environmental factors such as elevation may indirectly influence landslide occurrence by reflecting variations in relief energy, weathering processes and hydrological conditions at the regional scale [17].

Moreover, predisposing factors used in susceptibility modelling should capture spatial patterns associated with landslide distribution [18]. In this context, elevation can help discriminate between low-lying alluvial plains, where slope angles are generally low and landslide occurrence is limited, and higher relief sectors characterized by steeper valley sides and structural scarps, where gravitational processes are more active.

As shown in Figure 5, low elevation values (0–100 m) are mainly concentrated along the Tagus estuarine plain and coastal sectors, where Quaternary deposits and gentle slopes dominate. Intermediate altitudes (100–250 m) correspond to dissected sedimentary plateaus and valley

systems, whereas higher elevations (>300 m) are observed in structurally controlled sectors characterized by more resistant lithological units.

The use of 50 m elevation intervals allows the statistical evaluation of the relationship between elevation and landslide occurrence within the bivariate modelling framework, ensuring compatibility with the spatial resolution of the DEM and the regional scale of analysis.

2.3.3. ASPECT

Aspect represents the downslope direction of the maximum rate of change in elevation and describes the orientation of slope faces relative to the cardinal directions. It was derived from the 10 m resolution DEM using the Aspect tool in ArcGIS Pro (Spatial Analyst extension). The resulting raster expresses slope orientation in degrees and was subsequently reclassified into eight directional classes (North, Northeast, East, Southeast, South, Southwest, West and Northwest), with an additional class for flat areas (Figure 6).

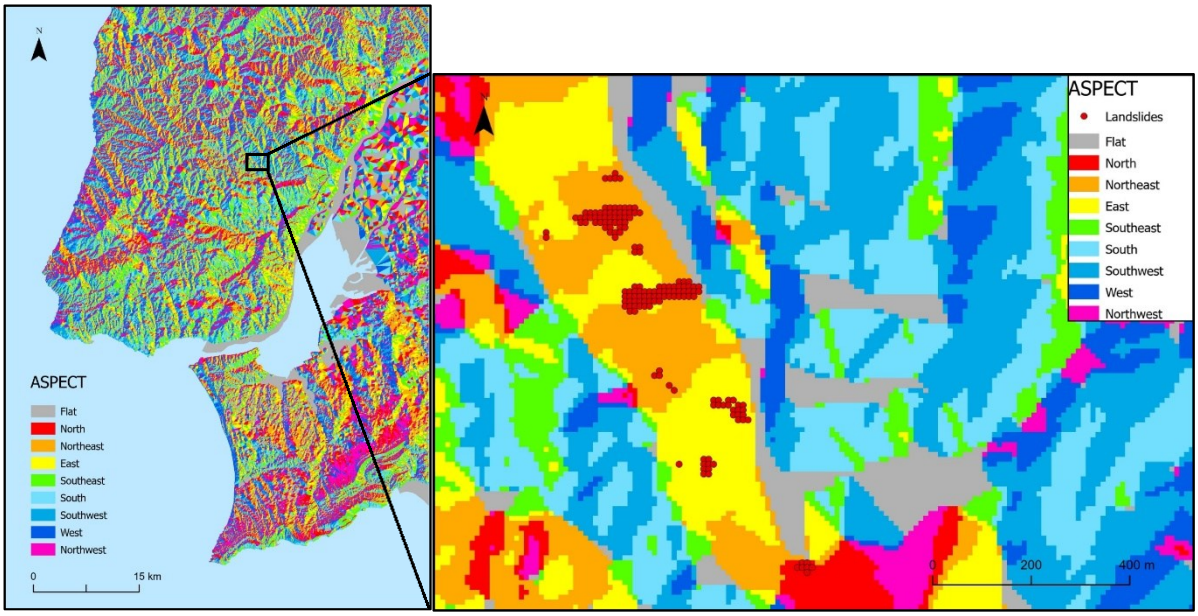

Figure 6: Aspect ratio map of the study area, subdivided into the different directional classes (left); detail of the map showing the overlap between the classes of the aspect map and the landslides of the inventory (right).

Aspect is commonly included as predisposing factor in landslide susceptibility modelling because it may influence microclimatic conditions, soil moisture distribution and vegetation patterns [17]. Differences in solar radiation exposure may lead to variations in evapotranspiration rates and soil water content, which in turn affect the mechanical behaviour of slope materials. In regions where rainfall-induced landslides dominate, slope orientation may control the persistence of soil saturation and the development of preferential infiltration pathways.

Morphometric parameters such as aspect are frequently included in statistical susceptibility models due to their indirect influence on slope hydrology and weathering processes and predisposing factors should reflect spatial patterns associated with landslide occurrence, particularly when analysing regional-scale datasets [17,18]. In this context, aspect may help explain variations in landslide frequency related to differential moisture retention and exposure to prevailing climatic conditions.

In the Lisbon region, the complex valley network and structural controls result in a highly heterogeneous spatial distribution of slope orientations. The alternation of north-facing and south-facing slopes along incised valleys may contribute to localized differences in soil moisture and weathering intensity, potentially influencing the spatial distribution of slope instability processes.

The classification into eight directional classes ensures compatibility with the bivariate statistical framework adopted in this study, allowing the evaluation of the relationship between slope orientation and landslide occurrence at the regional scale.

2.3.4. PLAN CURVATURE

Plan curvature describes the curvature of contour lines and represents the rate of change of aspect along the horizontal plane. It influences the convergence and divergence of surface runoff and therefore plays a significant role in controlling local hydrological processes. Plan curvature was derived from the DEM and initially computed at a spatial resolution of 50 m in order to reduce local noise effects often associated with curvature calculation at very fine resolutions. The resulting raster was subsequently resampled to a 10 m pixel resolution to

ensure spatial consistency with the remaining DEM-derived variables used in the susceptibility modelling process. Curvature values were classified into three morphometric categories based on their numerical range: concave surfaces (values < –0.05), rectilinear or planar surfaces (–0.05 to 0.05) and convex surfaces (values > 0.05) (Figure 7).

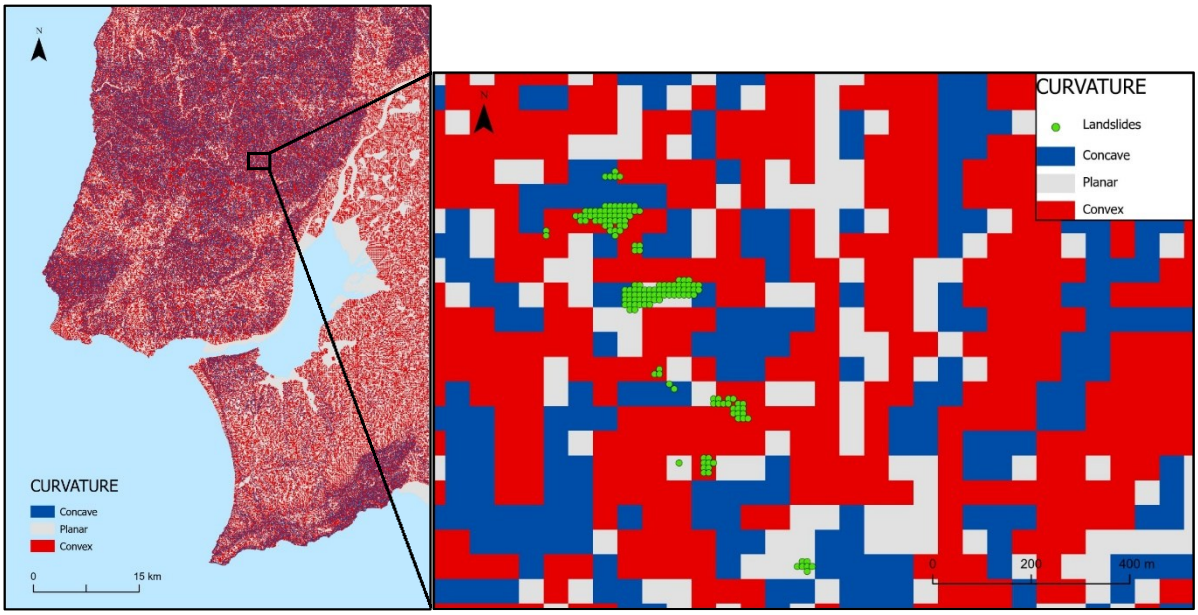

Figure 7: Plan curvature of the study area, subdivided into the Concave, Planar or Convex curvatures (left); detail of the map showing the ovrerlap between the classes of the Plan curvature map and the landslides of the inventory (right).

Concave surfaces (negative curvature values) are typically associated with flow convergence and water accumulation, favouring increased soil moisture and potential pore-water pressure development. Convex surfaces (positive curvature values) correspond to divergent flow conditions, where runoff is dispersed and soil moisture accumulation is generally lower. Planar areas represent transitional conditions with limited curvature influence.

Plan curvature is considered a relevant predisposing factor in landslide susceptibility modelling because it controls the spatial distribution of surface runoff convergence and divergence. By influencing the concentration of overland flow and subsurface water accumulation, curvature

directly affects local pore-water pressure conditions, which are critical in rainfall-induced slope failures [17,18].

In the Lisbon region, where landslides are predominantly triggered by rainfall events, the identification of concave sectors is particularly relevant. These areas often correspond to valley heads, hollows and convergent slopes where surface runoff is concentrated, and infiltration processes are enhanced. Conversely, convex ridge crests and spurs are generally associated with divergent flow patterns and comparatively lower water accumulation.

The classification into concave, planar and convex categories allows the statistical evaluation of the relationship between surface curvature and landslide occurrence within the adopted bivariate modelling framework, ensuring consistency with the regional scale of analysis and the spatial resolution of the DEM.

2.3.5. TOPOGRAPHIC WETNESS INDEX (TWI)

The Topographic Wetness Index (TWI) is a terrain-derived parameter that describes the spatial distribution of potential soil moisture as a function of upslope contributing area and local slope gradient. It was calculated from the DEM using the classical formulation:

$$TWI = \ln\left(\frac{a}{\tan\beta}\right)$$

where a represents the specific catchment area (flow accumulation per unit width) and β is the local slope angle [20].

The TWI raster was derived at the 10 m spatial resolution and subsequently classified into six classes using the standard deviation method (interval size = 1 standard deviation), ensuring that class thresholds reflect the statistical distribution of TWI values within the study area (Figure 8).

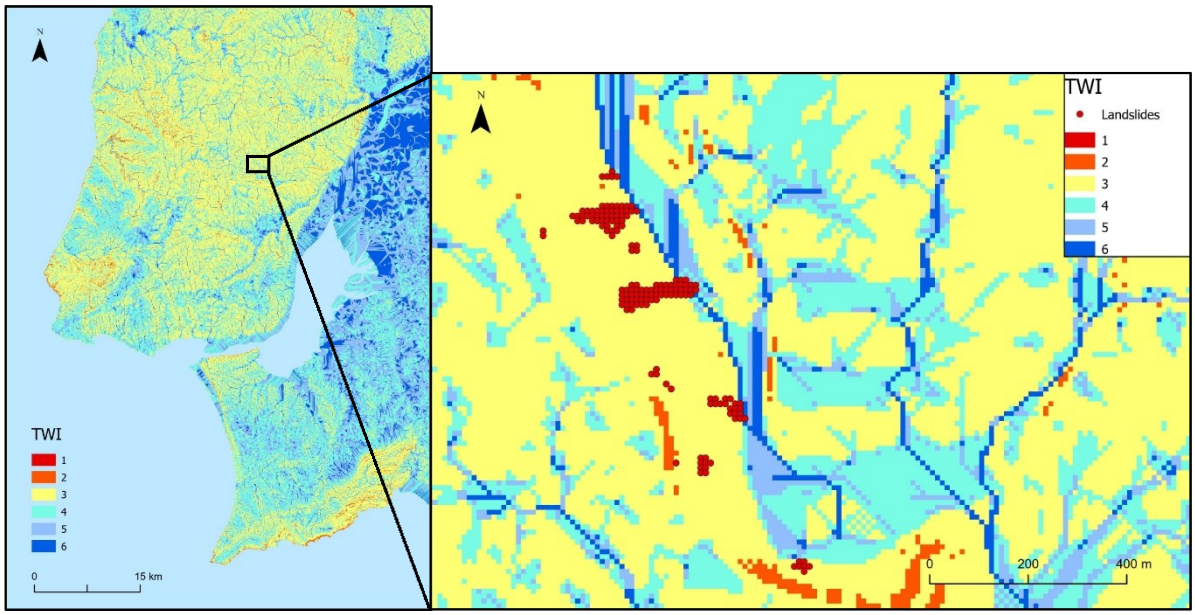

Figure 8: TWI map of the study area, subdivided into the six statistically defined classes (left); detail of the map showing the overlap between the classes of the TWI map and the landslides of the inventory (right).

The classification into six statistically defined classes (values of the TWI increase from class 1 to class 6, where class 6 shows the highest values) allows the evaluation of the relationship between increasing moisture potential and landslide occurrence within the adopted bivariate framework, maintaining coherence with the regional scale and DEM resolution.

TWI is widely recognized as a key hydrological predisposing factor in landslide susceptibility modelling [17]. By integrating slope gradient and contributing area, it identifies zones of potential water accumulation and soil saturation. High TWI values generally correspond to valley bottoms, convergent hollows and drainage lines, where surface runoff is concentrated and infiltration is enhanced. Low TWI values are typically associated with ridge crests and well-drained convex slopes.

In rainfall-induced landslide contexts, such as those documented in the Lisbon region, soil saturation and pore-water pressure increase play a fundamental role in slope failure initiation.

Therefore, TWI provides an indirect but physically meaningful representation of hydrological controls on slope instability.

2.3.6. TOPOGRAPHIC POSITION INDEX (TPI)

The Topographic Position Index (TPI) describes the relative elevation of a given cell compared to the mean elevation of its surrounding neighbourhood. It provides information on the local topographic position within the landscape, allowing the differentiation between ridge crests, slopes and valley bottoms. TPI was derived from the 10 m resolution DEM and calculated as the difference between the elevation of each cell and the average elevation of neighbouring cells within a defined analysis window.

Positive TPI values indicate locations that are higher than their surroundings (e.g., ridges or crests), whereas negative values correspond to areas lower than their surroundings (e.g., valley bottoms and depressions). Values close to zero generally represent mid-slope positions or relatively planar surfaces.

The resulting TPI raster was classified into six classes using the standard deviation method (interval size = 1 standard deviation), ensuring that the thresholds reflect the statistical distribution of values within the study area (Figure 9).

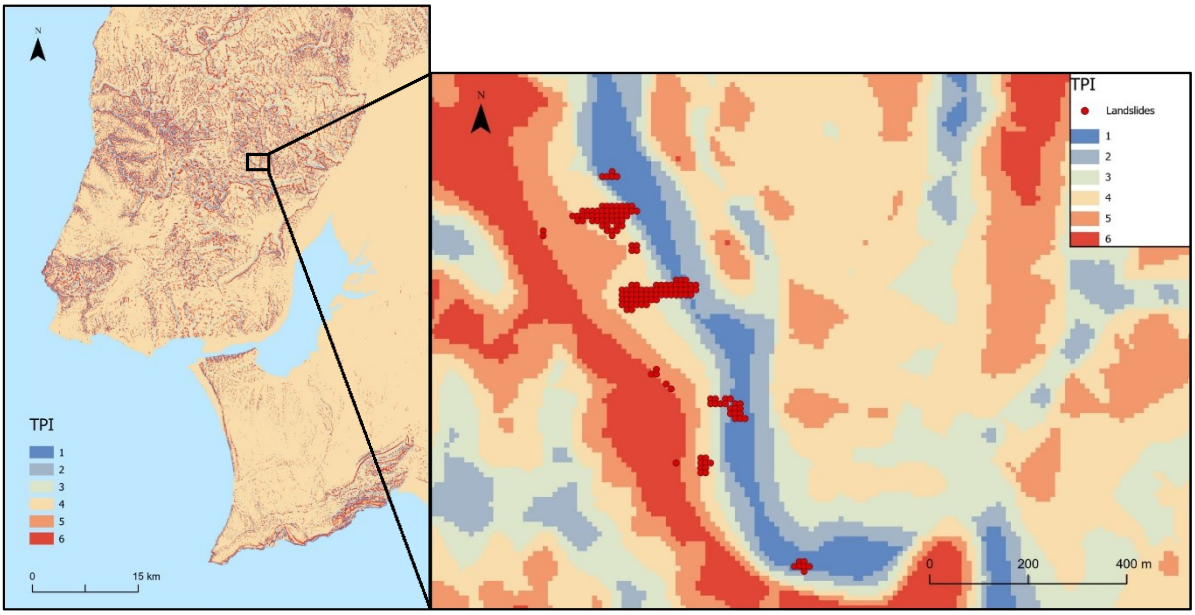

Figure 9: TPI map of the study area, subdivided into the six statistically defined classes (left); detail of the map showing the overlap between the classes of the TPI map and the landslides of the inventory (right).

This approach allows the identification of statistically distinct terrain positions without imposing arbitrary class boundaries.

TPI is considered a relevant predisposing factor in landslide susceptibility modelling because it captures terrain morphology at the mesoscale, complementing slope and curvature parameters [17]. While slope quantifies gradient and curvature describes surface concavity or convexity, TPI identifies the relative geomorphological setting of each pixel within the broader landscape structure. In rainfall-induced landslide contexts, valley bottoms and convergent lower slopes (negative TPI values) may be associated with higher soil moisture and sediment accumulation, whereas ridge crests (positive TPI values) typically exhibit divergent flow conditions.

In the Lisbon region, the incised valley network and structurally controlled relief result in pronounced contrasts between ridges, valley heads and mid-slope sectors. The inclusion of TPI therefore enhances the representation of terrain morphology and supports the evaluation of the

relationship between geomorphological position and landslide occurrence within the adopted bivariate modelling framework.

2.3.7. GEOLOGY

Geology represents one of the most significant predisposing factors in landslide susceptibility modelling, as lithological properties directly influence slope stability through variations in shear strength, permeability, weathering behaviour and structural discontinuities [17]. The selection of geological units in susceptibility models should reflect meaningful contrasts in mechanical and hydrogeological properties that may control the spatial distribution of landslides [18].

The geological dataset used in this study was derived from the official geological map at 1:25,000 scale (Figure 10). For susceptibility modelling purposes, each lithological unit represented in the original map legend (Figure 2) was considered as a separate class. This approach preserves the full lithological variability of the study area and allows the statistical method to identify specific geological units that exhibit stronger associations with landslide occurrence.

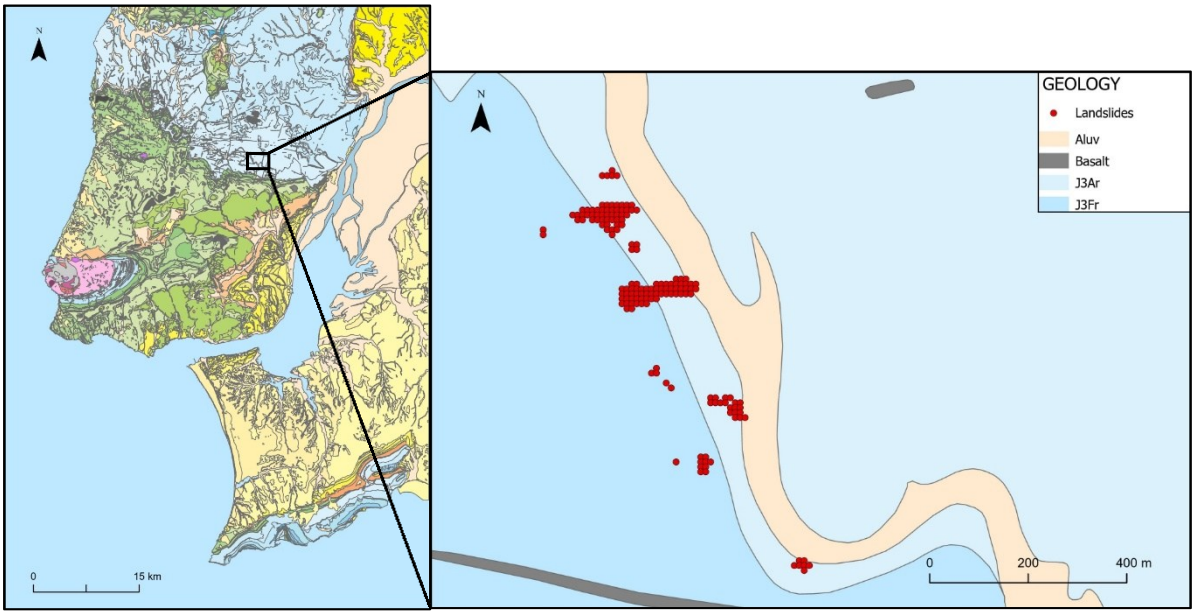

Figure 10: Geological map of the study area (left); detail of the map showing the overlap between the classes of the Geological map and the landslides of the inventory (right). The corresponding lithologies for each code are provided in Annex 5 in the Annex section.

However, for descriptive and interpretative purposes, the detailed lithological units were grouped into broader chronostratigraphic domains, following the standard colour scheme of the chronostratigraphic map as follows:

a) Cenozoic units (yellow and pink tones), including Neogene formations (darker yellow shades) and Quaternary deposits (lighter yellow shades). These units are widely distributed across the study area, particularly in the Lower Tagus Basin and along alluvial plains. They are predominantly composed of unconsolidated to weakly consolidated sediments such as sands, clays, marls and conglomerates, which may exhibit reduced shear strength and high susceptibility to saturation.

b) Cretaceous units (green tones), consisting mainly of carbonate and mixed sedimentary formations, locally associated with volcanic materials. These lithologies form a significant portion of the regional substratum and often display variable mechanical behaviour depending on fracturing and weathering intensity.

c) Jurassic units (blue and light-blue tones), composed largely of limestones, marls and associated sedimentary sequences belonging to the Lusitanian Basin. These formations frequently exhibit structural control through bedding planes and fault systems, which may act as preferential failure surfaces.
d) Triassic units (purple tones), occurring locally and generally composed of older sedimentary sequences with distinct lithological and structural characteristics.
e) Magmatic rocks (grey tones), including intrusive and volcanic units such as basalts and related igneous formations. These rocks typically present higher mechanical strength but may locally contribute to instability where intense fracturing or weathering is present.

This dual-level approach ensures methodological consistency: the statistical modelling benefits from the detailed lithological classification, while the aggregation into broader stratigraphic groups facilitates geological interpretation and maintains coherence with the regional geological framework described in Chapter 1.

In the Lisbon region, landslide activity is frequently associated with fine-grained sedimentary formations and lithological contrasts within the sedimentary sequences, which may locally reduce shear strength and favour slope instability under rainfall-induced conditions. The inclusion of geology as an independent variable therefore provides a fundamental representation of material properties and structural controls influencing slope failure processes.

2.3.8. SOIL TYPE

Soil type represents a key predisposing factor in landslide susceptibility modelling, as soil properties directly influence shear strength, permeability, plasticity and drainage behaviour. Variations in grain size distribution, clay content and degree of weathering may significantly affect slope stability, particularly under rainfall-induced conditions [17].

The soil dataset used in this study was derived from the official soil map at 1:25,000 scale (Figure 11).

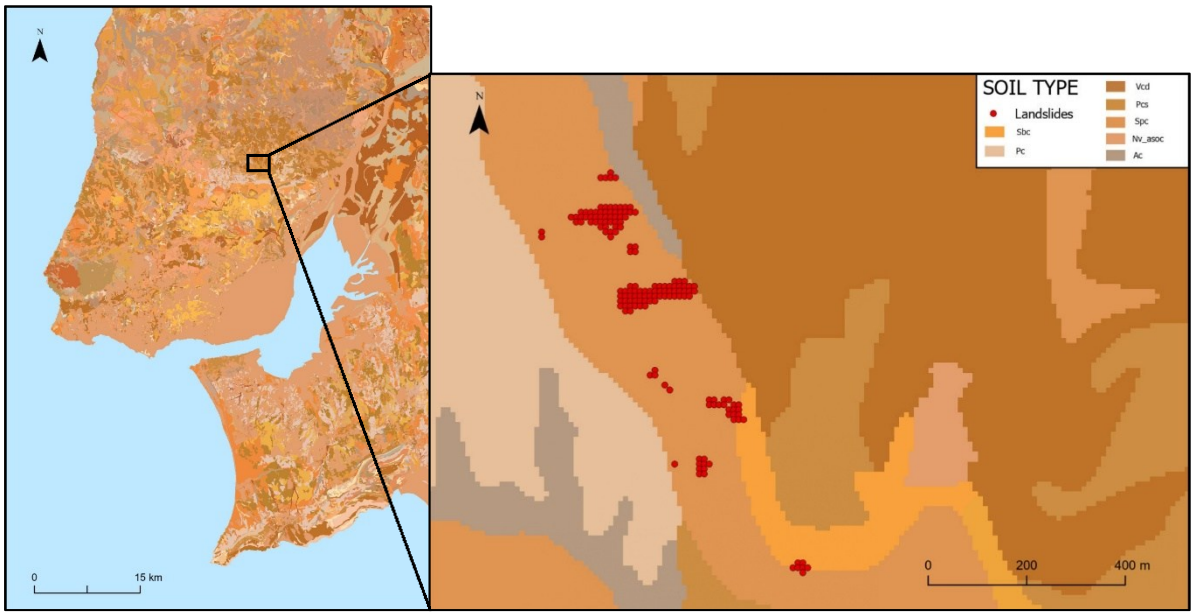

Figure 11: Soil type map of the study area (left); detail of the map showing the overlap between the soil type classes and the landslides of the inventory (right).

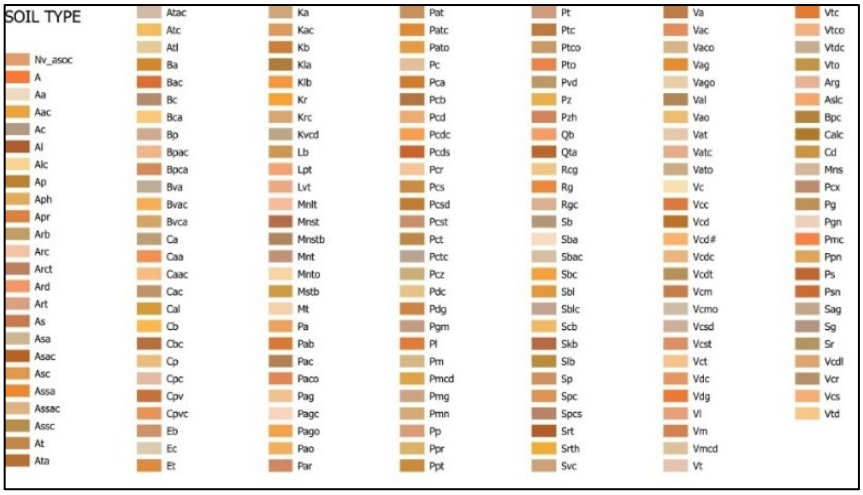

Figure 12: Legend of the soil type map (Figure 11); the codes are translated inside Annex 6 in the Annex section.

For susceptibility modelling purposes, each soil unit represented in the original legend (Figure 12) was treated as an individual class. This approach preserves the pedological variability of

the study area and allows the statistical analysis to identify specific soil types more frequently associated with landslide occurrence.

The mapped soil units include a wide range of pedological classes developed over sedimentary and magmatic substrates, reflecting the geological and geomorphological heterogeneity of the Lisbon region. These soils vary from well-drained sandy or loamy profiles to clay-rich and poorly drained units, as well as shallow soils developed over resistant lithologies. Clay-rich and fine-textured soils may exhibit reduced permeability and higher susceptibility to water retention, potentially favouring the development of elevated pore-water pressures during prolonged rainfall events. Conversely, coarse-textured or well-drained soils may facilitate rapid infiltration and drainage, although instability may still occur where soil thickness and slope gradient are significant.

Given the strong relationship between rainfall and landslide occurrence in the Lisbon region, soil hydraulic behaviour plays a crucial role in slope response to rainfall. The inclusion of soil type as an independent variable therefore provides a complementary representation of near-surface material properties that are not fully captured by lithology alone.

Although numerous soil units are represented in the dataset, their use as individual classes in the bivariate modelling framework ensures that the statistical method can objectively determine which pedological conditions exhibit stronger associations with mapped landslides.

2.4. BUILDINGS DATASET AND POPULATION DATA

The assessment of exposed elements was based on detailed spatial datasets describing buildings' locations and resident population. In landslide risk analysis, buildings and population represent two of the most relevant exposed elements, as they directly relate to potential physical damage and human losses [21].

The buildings dataset consists of a georeferenced inventory of individual building points (centroids), each associated with municipal administrative codes, enabling aggregation at the municipal scale (Figure 13). Resident population data were obtained from census records originally reported at the level of statistical subsections.

For the multitemporal analysis, building and resident population datasets from 2011 and 2021 were used to quantify changes in exposure over the decade 2011–2021. This approach supports the assessment of how changes in the built environment and population distribution may modify landslide exposure over time [22].

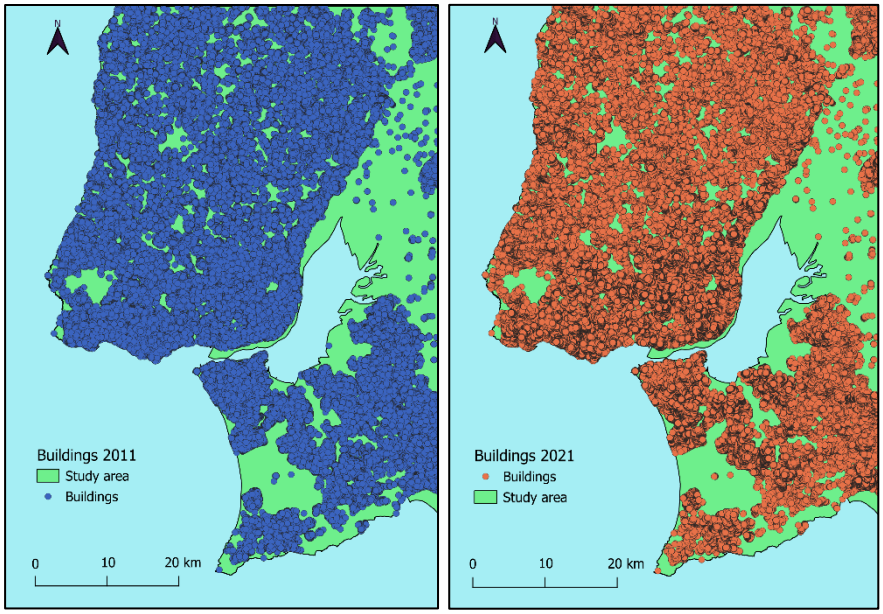

Figure 13: Buildings datasets of 2011 (left) and 2021 (right).

To improve the spatial representation of population, resident population totals at the census subsection level were redistributed to individual buildings using a dasymetric mapping approach [19]. Within each subsection, census population was disaggregated and allocated across building centroids, producing a building-level proxy of resident population distribution. This procedure enables the estimation of exposed residents by intersecting the redistributed population data with the LSM.

By intersecting these exposure datasets with the LSM, it becomes possible to quantify:

a) the number of buildings within each susceptibility class,
b) the resident population potentially exposed within each susceptibility class,
c) and changes in exposed elements between 2011 and 2021.

It is important to emphasize that high susceptibility does not automatically imply high risk. As previously discussed, risk emerges when susceptible areas coincide with significant exposure and vulnerable elements. Therefore, analysing the spatial distribution and temporal evolution of buildings and resident population is fundamental for understanding how exposure to landslides may evolve over time in the Lisbon region.

2.5. ROAD NETWORK DATA

Transportation infrastructure represents a critical exposed element, as road interruptions may generate significant economic losses, accessibility constraints and cascading socio-economic impacts [21]. In municipal-scale studies, the road network is particularly relevant because it connects residential areas, industrial zones and public services, and its disruption may isolate communities during emergency situations.

The road network dataset used in this study was derived from OpenStreetMap and includes all mapped road segments within the study area as shown in Figure 14. Each road segment is georeferenced and attributed with a functional classification (motorway, trunk, primary, secondary and tertiary).

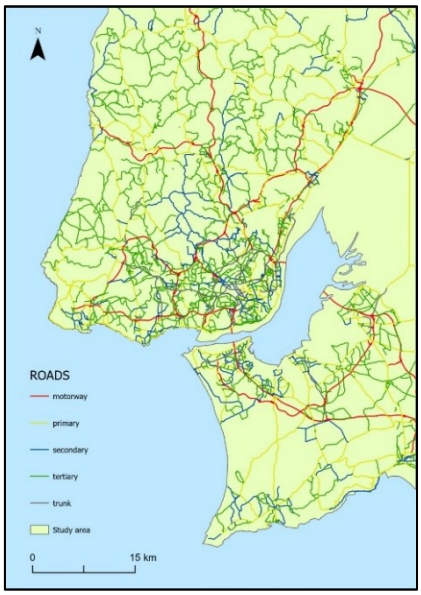

Figure 14: Roads subdivided into the different segment types.

For each municipality, the total road length (in kilometres) was calculated by summing the length of individual road segments. In addition, the number of road segments belonging to each functional class was computed, allowing the characterization of infrastructure density and typological composition at the municipal scale (Annex 1). This aggregation enables the identification of municipalities with more extensive and hierarchically complex transportation networks.

Road exposure assessment is particularly important in rainfall-induced landslide contexts, where slope failures may obstruct critical transportation corridors. As highlighted in previous research, infrastructure located in landslide-prone areas may experience recurrent damage and service disruption, increasing indirect economic losses and emergency response difficulties [21]. Therefore, integrating the road network dataset with the LSM allows the quantification of:

a) the total length of roads located within each susceptibility class,
b) the exposure of higher-hierarchy roads (e.g., motorways and primary roads),
c) and the potential impact of road disruption in municipalities highly dependent on specific transport corridors.

CHAPTER 3: METHODOLOGY

A landslide susceptibility map subdivides the terrain into zones with differing likelihoods that landslides of a certain type may occur. Landslide susceptibility assessment can be considered the initial step towards a landslide hazard and risk assessment, but it can also be an end product in itself that can be used in land-use planning and environmental impact assessment [18].

The methods used for landslide susceptibility analysis are usually based on two assumptions. The first is that past conditions are indicative of future conditions. Therefore, areas that have experienced landslides in the past are likely to experience them in the future too, as they maintain similar environmental settings (e.g. topography, geology, soil, geomorphology and land use) [18].

Overviews of the methods available for landslide susceptibility assessment can be found in literature and are shown in Figure 15 [23–29]; these methods, are both qualitative (inventory-based and knowledge-driven methods) and quantitative (data-driven methods and physically based models). Inventory-based methods are required as a prelude to all other methods, as they provide the most important input and are used to validate the resulting maps [18].

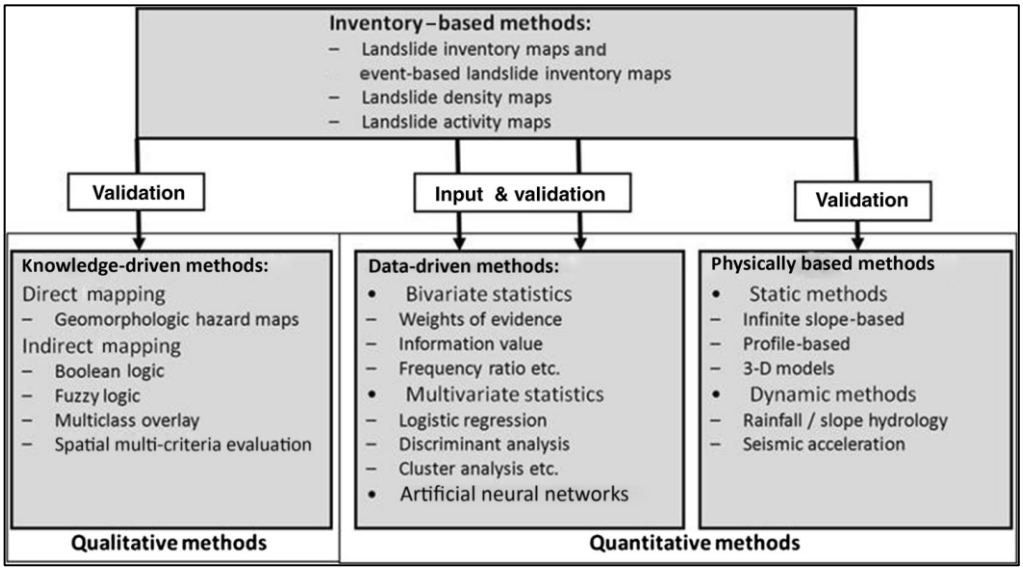

Figure 15: Methods for landslide susceptibility assessment.

The methodological framework adopted in this study aims to assess landslide susceptibility and to quantify the exposure of buildings, resident population and road infrastructure within the study area. The workflow integrates geomorphological analysis, statistical modelling and spatial overlay techniques within a GIS environment (Figure 16). The approach is structured into five main phases:

a) Derivation of independent variables from topographic, geological and soil type datasets.
b) Calculation of Information Value (IV) scores using a bivariate statistical method.
c) Training and validation of susceptibility models through inventory partitioning and cross-validation.
d) Generation and classification of the final LSM.
e) Spatial intersection between susceptibility classes and exposed elements (buildings, population and roads) to evaluate municipal-scale exposure.

The susceptibility modelling is based on a bivariate statistical method which quantifies the statistical relationship between landslide occurrence and predisposing factors through the computation of I V scores [30]. The landslide inventory was divided into three equal subsets, enabling a three-fold cross-validation procedure that enhances the robustness and predictive reliability of the models.

The predictive performance of each model was evaluated using Prediction-rate Curves and the Area Under the Curve (AUC), following established validation approaches [31,32]. The final susceptibility map was obtained by averaging the IV-based susceptibility scores of the validated models and defining susceptibility thresholds based on the cumulative distribution of landslide-covered area.

Subsequently, the susceptibility map was reclassified into operational classes and intersected with spatial datasets representing buildings, resident population and road infrastructure. This step enables the quantification of exposed elements within the highest susceptibility classes and supports the analysis of the spatial and temporal evolution of exposure and potential changes in landslide risk at the municipal scale.

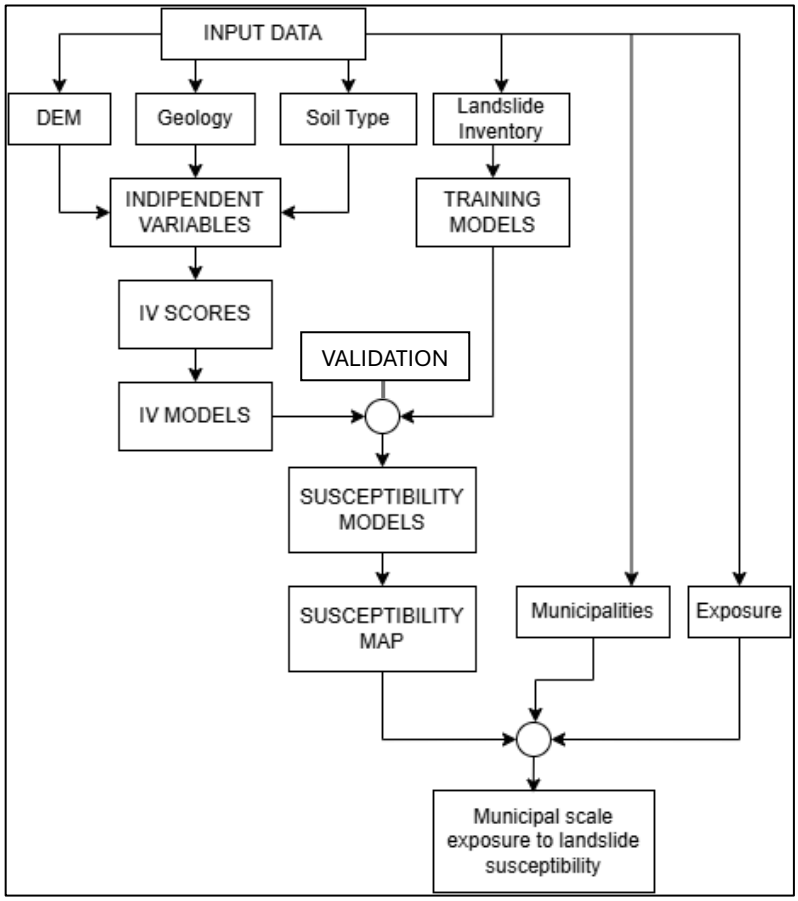

Figure 16: Flowchart of the methodology process.

3.1. INFORMATION VALUE MODELLING

To quantify the relationship between landslide occurrence and the independent variables, the Information Value (IV) method was applied. The IV approach is a bivariate statistical technique widely used in landslide susceptibility assessment [30], [33–35].

Following a cross-validation strategy, the landslide inventory was randomly divided into three equal subsets (approximately 33.3% each), labelled A, B and C. These subsets were then combined in pairs to generate three independent training datasets (AB, AC and BC). For each training model, the remaining subset was used for validation (e.g., model AB validated with C). This rotation procedure ensured that all landslide cases were used both for calibration and

independent validation, providing a more robust assessment of predictive performance and potential overfitting, in line with best practices for susceptibility modelling [35].

All independent variables were previously reclassified into discrete classes. Elevation was classified using fixed intervals up to 500 m, corresponding to the maximum altitude of the study area. For each training dataset, every independent variable was cross tabulated with the corresponding landslide subset. This procedure generated two essential parameters for each class of each variable:

Value_1: area of the class affected by landslides

Value_0: area of the class not affected by landslides

These values allowed the computation of the Information Value score for each variable class using the formulation proposed by Yin and Yan (1988):

$$IV_i = \ln\left(\frac{S_i/N_i}{S/N}\right)$$

where:

$S =$ total landslide area in the training model ($\sum$ Value_1)

N = total area of the study area (landslide + non-landslide areas)

S_i = landslide area within class i (Value_1)

N_i = total area of class i (Value_1 + Value_0)

This formulation expresses the logarithmic ratio between the conditional probability of landslide occurrence within a given class and the prior probability of landslide occurrence in the entire study area. Positive IV values indicate that a class is more susceptible than average, whereas negative values indicate lower susceptibility [30,35].

For each terrain unit (10 × 10 m grid cell), the final susceptibility score was obtained by summing the IV scores of all corresponding variable classes. This additive property of IV models allows the integration of multiple predisposing factors while preserving the individual contribution of each variable class [33,34].

The resulting susceptibility maps derived from the three training combinations (AB, AC, BC) were subsequently validated using the respective independent subset, enabling an objective assessment of predictive performance.

3.2. VALIDATION OF THE SUSCEPTIBILITY MODELS

After the computation of the Information Value (IV) scores for each independent variable and for each paired training inventory (AB, AC, BC), the final IV score for every class was calculated as the mean IV value obtained across the three training models. This averaging procedure reduces potential bias related to the random partitioning of the landslide inventory and ensures a more robust estimation of the contribution of each predisposing factor.

Since IV scores are calculated using a natural logarithm formulation, invalid values may occur when the logarithmic argument equals zero (i.e., when $S_i = 0$). To avoid missing values during raster processing, each invalid IV value was replaced with a fixed value equal to one centesimal lower than the minimum IV value within the corresponding variable. This conservative adjustment preserves the statistical hierarchy of the classes while preventing computational errors during raster algebra operations.

The computed IV scores were then joined to the attribute tables of the corresponding independent variables. Using the *Lookup* tool in ArcGIS Pro, individual IV raster layers were generated for each predisposing factor and for each paired training inventory (e.g., slope_IV_AB, TWI_IV_AB, etc.).

The final susceptibility model for each paired inventory was obtained through raster algebra using the *Raster Calculator* tool:

$$LS_{AB} = IV_{aspect,AB} + IV_{plan\,curvature,AB} + IV_{elevation,AB} + IV_{slope,AB} + IV_{TPI,AB} + IV_{TWI,AB} + IV_{geology,AB} + IV_{soil,AB}$$

The same procedure was applied to generate the AC and BC susceptibility models.

To preserve decimal precision during subsequent spatial operations, each susceptibility raster was multiplied by 1000 and converted to integer format. This scaling step avoided loss of precision in later tabulation and reclassification procedures.

The predictive performance of each susceptibility model was assessed using an independent validation subset. For example, the susceptibility model generated from training inventory AB was validated using subset C. This rotation procedure guarantees independent testing and follows best practices in landslide susceptibility modelling.

Each susceptibility raster was cross tabulated with the corresponding validation subset. The resulting table included:

- Information value score,
- Value_0: area (m²) without landslides,
- Value_1: area (m²) with landslides.

From these values, cumulative percentages of correctly predicted landslide area were calculated, allowing the construction of a Prediction-Rate Curve, which provides a graphical assessment of how effectively the model concentrates validation landslides within the highest susceptibility classes[32].

The Area Under the Curve (AUC) was calculated from the prediction-rate curve as a synthetic measure of model predictive performance [22], [27].

$$AAC = \sum_{i=1}^{n} \left[\left(Lsi - Li \right) * \frac{ai + b1}{2} \right]$$

Where:

(Lsi – Li): class amplitude

ai: value of the ordinate corresponding to Li

b1: value of the ordinate corresponding to Lsi.

AUC values range from 0.5, indicating random prediction, to values approaching 1, indicating excellent discrimination capacity. Following [22], model performance may be interpreted as acceptable for AUC > 0.75, satisfactory for AUC > 0.80 and accurate for AUC > 0.90 [31].

Finally, the susceptibility scores obtained from the three validated models were combined to produce the final LSM, which was subsequently classified using thresholds based on the cumulative distribution of landslide-covered area.

3.3. SUSCEPTIBILITY THRESHOLDS AND FINAL SUSCEPTIBILITY MAP

After the validation of the three paired training models (AB, AC and BC), all models demonstrated high predictive performance, with AUC values equal to or higher than 0.90, indicating accurate discrimination capacity (Figure 17).

The final susceptibility model was obtained by calculating the mean IV score for each independent variable class across the three training models. This averaging procedure ensures that the final model integrates the statistical contribution of each predisposing factor class while minimizing variability introduced by inventory partitioning.

The final LSM was subsequently cross-tabulated with the complete landslide inventory in order to generate the corresponding Success-Rate Curve and compute the final AUC value. These results confirm the strong predictive performance of the final model. Since the IV-based susceptibility model produces a continuous range of values, it was necessary to define threshold values to generate discrete susceptibility classes suitable for spatial interpretation and exposure assessment.

3.4. EXPOSURE ASSESSMENT

The exposure assessment was performed by integrating the final LSM with spatial datasets representing buildings, resident population and road infrastructure. According to widely accepted risk assessment frameworks, exposure corresponds to the spatial overlap between susceptible areas and elements at risk, including population, buildings and critical infrastructure [21,22]. In this study, exposure is evaluated after the definition of susceptibility classes, thus allowing the identification of assets potentially affected by future landslide events.

Starting from the five susceptibility classes previously defined through IV-based thresholds, the raster was reclassified in ArcGIS Pro into a binary susceptibility map for exposure analysis (Figure 18).

The binary susceptibility raster was converted into a polygon shapefile and spatially intersected with:

a) the buildings and resident population datasets (2011 and 2021),
b) the road infrastructure dataset (Figure 14).

Through spatial overlay analysis, each building (points) and each road segment (line feature) was overlaid with the landslide susceptible areas. This procedure allowed the quantification of:

a) the number of buildings located within susceptible areas,
b) the number of residents potentially exposed within susceptible areas,

c) the total length of roads falling within susceptible areas.

Similarly, the inclusion of road infrastructure emphasise the importance of transportation networks, not only as exposed assets but also as critical components for emergency response and accessibility [21,22].

The availability of building and resident datasets for both 2011 and 2021 allowed a multitemporal comparison of exposure patterns. By applying the same susceptibility thresholds to both datasets, it was possible to evaluate how urban expansion and demographic evolution may have influenced the spatial distribution of exposed elements over time.

3.5. TEMPORAL ANALYSIS OF EXPOSURE CHANGES (2011-2021)

The temporal analysis of exposure was conducted by comparing the spatial distribution of buildings and resident population intersecting the landslide susceptible areas (which integrates the very high, high and moderate susceptibility classes previously defined) in 2011 and 2021. The same susceptibility thresholds and binary classification were applied to both temporal datasets in order to ensure methodological consistency and comparability.

CHAPTER 4: RESULTS

4.1. INTERPRETATION OF THE IV SCORES

Table 1 presents the ranking of the independent variables based on the mean IV scores and on the three paired training models (AB, AC and BC). The comparison allows the evaluation of the relative contribution and statistical stability of each predisposing factor across different inventory combinations.

Table 1: Ranking of the most influential independent variables based on the IV scores.

Variable	IV Model Mean	IV AB Model	IV AC Model	IV BC Model
Slope > 45º	2.980	2.924	2.982	3.036
Kvcd	2.942	3.628	3.614	1.5842
40º < Slope < 45º	2.631	2.489	2.662	2.742
J3Ab	2.495	2.462	2.558	2.464
J3Q	2.286	2.614	1.886	2.3565
Vcd#	2.171	2.472	2.3428	1.6984
Vcr	1.389	-1.636	2.833	2.972
J1VS	-0.078	3.321	-6.980	3.422
Ba	0.998	-1.556	2.192	2.359
TWI Class 2	1.557	1.523	1.593	1.5549
TPI Class 1	1.378	1.328	1.371	1.4355
Elevation (200-250m)	1.301	1.328	1.362	1.2141
Elevation (250-300m)	1.168	1.193	1.098	1.2137
TPI Class 2	0.837	0.910	0.863	0.7388

TWI Class 3	0.704	0.699	0.708	0.7041
Concave Curvature	0.697	0.697	0.712	0.6810
Aspect Northeast	0.556	0.555	0.560	0.5519
Aspect North	0.440	0.484	0.310	0.5257
Aspect East	0.362	0.327	0.304	0.4538
Convex Curvature	0.010	-0.007	0.020	0.0175

The results indicate that slope-related variables represent the most influential predisposing factors in all models. In particular, *Slope > 45º* shows the highest mean score (2.980) and consistently high values across AB (2.924), AC (2.982) and BC (3.036). Similarly, *40º < Slope < 45º* maintains elevated values in all training models. This confirms that slope gradient is a primary geomorphological control on landslide occurrence within the study area, coherently with its mechanical role in gravitational instability processes.

Among the thematic variables, several soil classes exhibit high IV scores. Clay-rich vertic soils (*Kvcd*) presents one of the highest contributions overall, especially in AB (3.628) and AC (3.614), while red vertic soils (*Vcr*) also shows strong influence in AC (2.833) and BC (2.972). These results highlight the importance of soil-related material properties in controlling slope stability, suggesting that specific soil units are statistically associated with higher landslide occurrence than others.

Regarding geological units, classes such as *J3Q* (limestones), *J1VS* (volcano-sedimentary complex) and *J3Ab* (marls and mudstones) show relatively high and stable values across the models, particularly in AB and BC. Although some variability exists between paired inventories, geology consistently ranks among the most relevant predisposing factors, suggesting that lithological and structural characteristics are closely associated with the observed susceptibility patterns.

Hydrological–morphometric indices, including TWI and TPI, display intermediate but remarkably stable contributions. The *TWI Class 2* maintains values around 1.55 in all models, while *TPI Class 1* and elevation classes show moderate and consistent influence. This suggests that topographic control on water accumulation and relative position within the landscape contributes to landslide predisposition, although with lower explanatory power than slope and selected soil or geological units.

Conversely, aspect and curvature classes generally present lower IV scores. While *Concave Curvature* and *Northeast Aspect* show small but consistent positive values, their contribution remains limited compared to other factors. The class *Convex Curvature* displays values close to zero (and slightly negative in AB), indicating a negligible influence in discriminating between landslide and non-landslide prone areas.

Overall, the comparison among AB, AC and BC models demonstrates a strong coherence in the ranking of the most influential variables, particularly for slope, selected soil classes and geology. The limited variability across training subsets supports the robustness of the model and confirms that the identified predisposing factors consistently explain the spatial distribution of landslides within the study area.

4.2. VALIDATION OF THE SUSCEPTIBILITY MODELS

All three paired models (Model AB, Model AC and Model BC) achieved AUC values equal to or higher than 0.90, indicating high predictive performance (Figure 17, 18, 19).

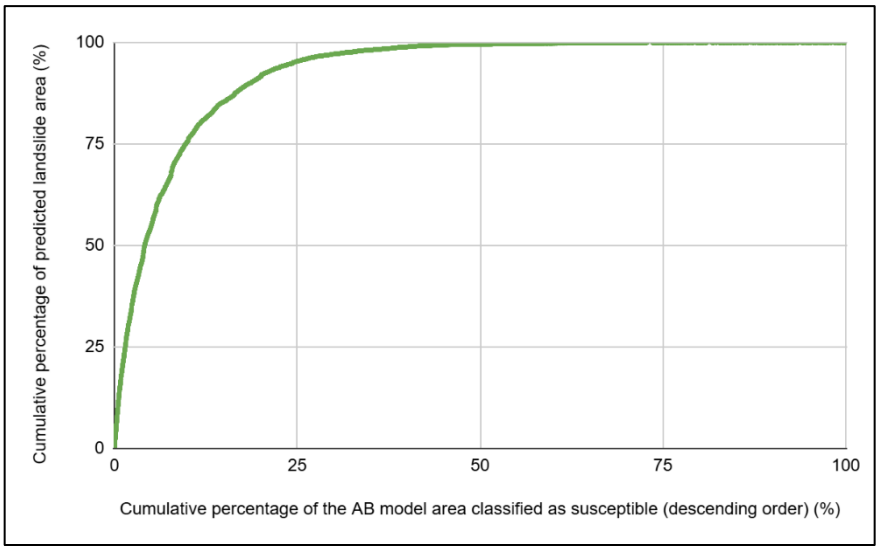

Figure 17: Success-rate curve for the AB susceptibility model (IV AB values).

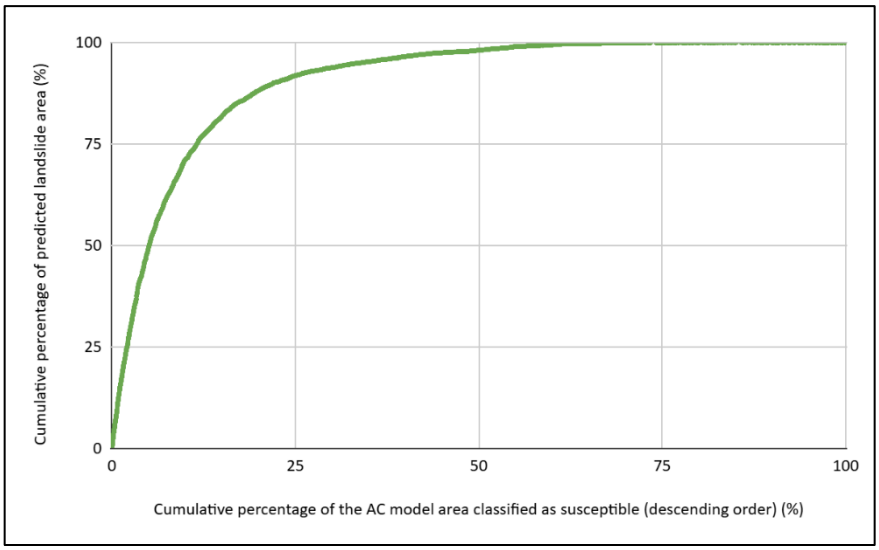

Figure 18: Success-rate curve for the AC susceptibility model (IV AC values).

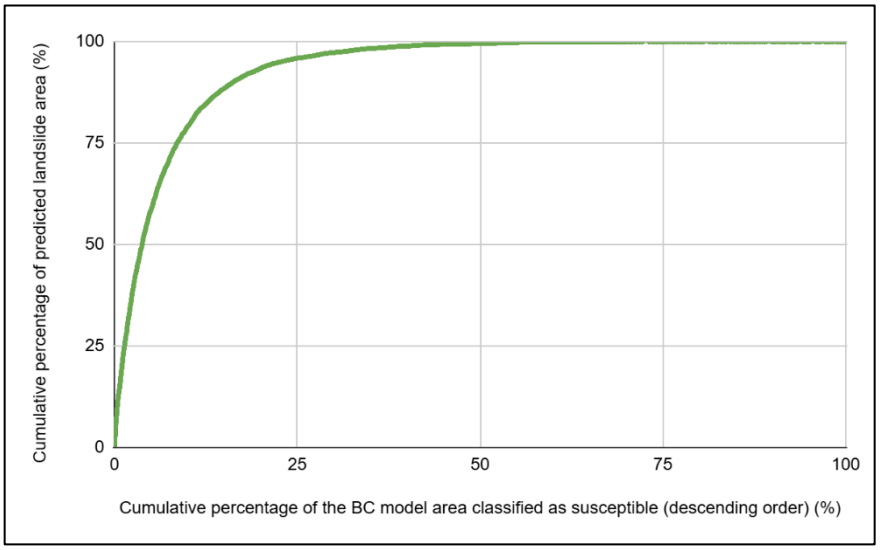

Figure 19: Success-rate curve for the BC susceptibility model (IV BC values).

These results confirm the robustness of the Information Value approach and demonstrate that the predisposing factors consistently explain the spatial distribution of landslides across different inventory partitions.

The final susceptibility model, obtained by averaging the IV scores across all training combinations, also yielded an AUC value above 0.90 when evaluated against the complete inventory. The Success-Rate Curve of this final model (Figure 20) confirms its strong performance, with a steep initial slope indicating that a large proportion of landslides is concentrated within a relatively small fraction of the study area.

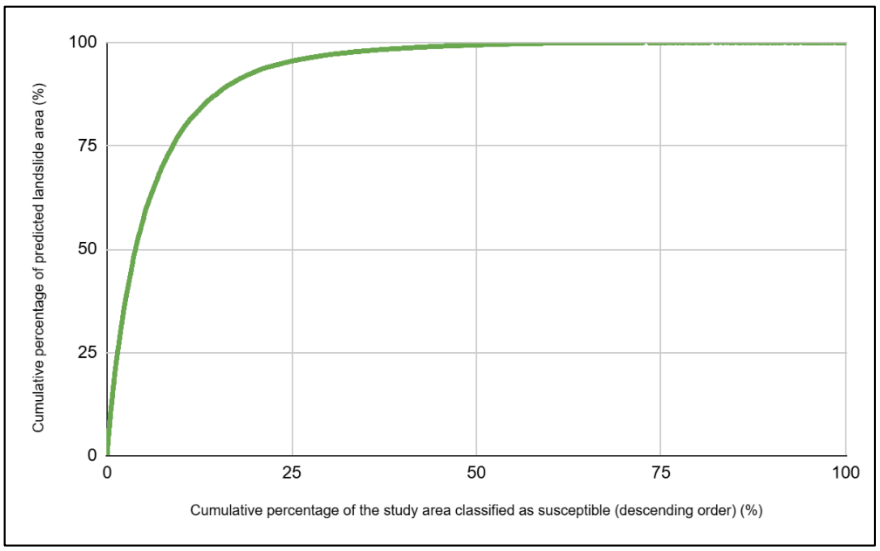

Figure 20: Success-rate curve for the final susceptibility model (IV mean values).

The obtained AUC values therefore classify all models, and particularly the final susceptibility model (IV mean values), as accurate susceptibility models.

The validation results of the final susceptibility model were subsequently used to determine the operational susceptibility thresholds. The cumulative distribution of landslide-covered area was analysed to identify the IV values corresponding to 50%, 70%, 90%, 95% and 100% of total landslide area. These threshold values represent the breakpoints used to convert the continuous susceptibility raster into discrete classes.

The most relevant result is that 90% of the total landslide-covered area is concentrated within only 16.75% of the study area.

This high concentration confirms the strong efficiency of the model and justifies the selection of the 90% threshold for subsequent exposure analysis (Table 3).

4.3. LANDSLIDE SUSCEPTIBILITY MAP

Following the validation phase and the definition of statistically derived thresholds, the continuous IV-based susceptibility raster was reclassified into six discrete susceptibility classes according to the cumulative distribution of landslide-covered area. The resulting map (Figure 21) illustrates the spatial distribution of susceptibility levels across the study area.

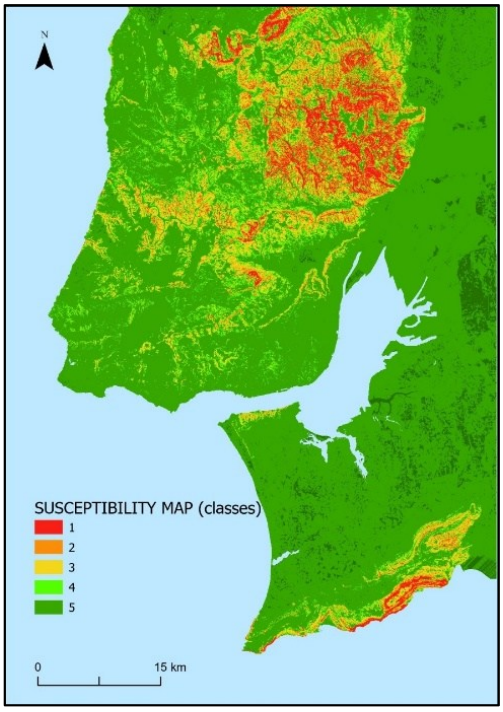

Figure 21: Final landslide susceptibility map, subdivided into five susceptibility classes (1=very high susceptibility; 5=low susceptibility).

The five classes were defined using performance-based breakpoints corresponding to 50%, 70%, 90%, 95% and 100% of cumulative landslide area, as described in the methodological framework. These thresholds are not arbitrary but are derived from the validation table of the final susceptibility model (IV mean values), ensuring that each class reflects a quantifiable concentration of historical landslide occurrences (Table 2).

Table 2: Definition of susceptibility classes based on Information Value score ranges and cumulative percentages of total area and landslide area

Susceptibility class	IV score range (descending order)	Cumulative % of total area	Cumulative % of landslide area
Very High	5,285	0-3.83	50
High	4,018	3.83-7.45	70
Moderate	1,537	7.45-16.75	90
Low	-123	16.75-23.78	95
Very Low	-18,664	23.78-95.38	100

The spatial pattern of the six-class map shows a clear concentration of very high and high susceptibility (Classes 1 and 2) in:

a) structurally controlled and morphologically dissected sectors,
b) steep slopes and valley flanks,
c) coastal escarpments in the southern portion of the study area.

Intermediate susceptibility (Class 3) forms transitional belts surrounding the highest classes, while low and very low susceptibility (Classes 4–6) dominate the gently sloping plains and less dissected terrains.

The efficiency of the classification is confirmed by the strong spatial clustering of historical landslides within the first three classes, which collectively account for 90% of total landslide-covered area within only 16.75% of the study area. This reflects a high discriminatory power of the model and a strong concentration index.

This classification scheme ensures that susceptibility classes are directly linked to the spatial concentration of landslides rather than arbitrarily defined intervals. The resulting map provides a spatially explicit representation of landslide susceptibility across the study area and constitutes the basis for the subsequent exposure assessment of buildings, population and road infrastructure at the municipal scale.

For exposure assessment purposes, the five-class susceptibility map was further reclassified into two operational classes, only covering the very high (Class 1) and high (Class 2) susceptibility (Figure 22).

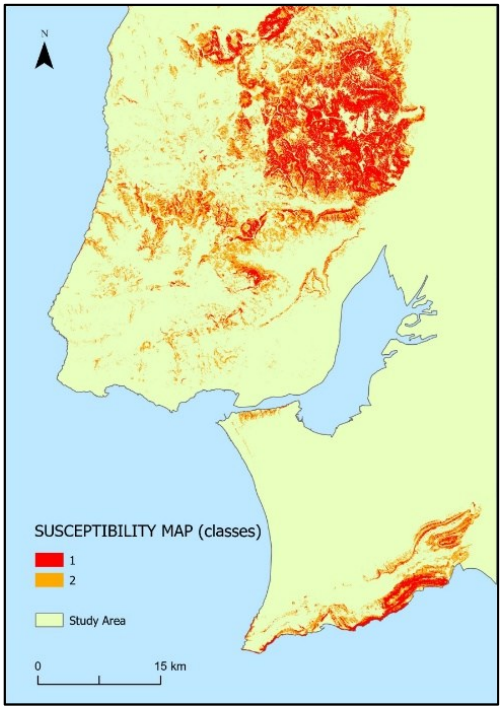

Figure 22: Susceptibility map subdivided into two classes, identifying only the most critical classes.

The Very High and High susceptibility classes were merged into a single susceptible class (Class 1), while the Moderate susceptibility class was left undisturbed (Class 2). This final configuration captures 90% of the total landslide-covered area within 16.75% of the study area, indicating high predictive efficiency of the model.

Although a 70% landslide-covered area threshold is commonly adopted in susceptibility studies to balance omission and commission errors, higher thresholds may result in a broader delineation of susceptible terrain.

As shown in Figure 21, high-susceptibility areas form continuous belts along steep slopes, structural alignments and coastal cliffs, while low-susceptibility areas dominate flatter inland sectors.

The decision to adopt the 90% cumulative threshold, is justified by the model performance: capturing 90% of landslides within only 16.75% of the total area ensures a high level of predictive efficiency without excessively enlarging susceptible zones.

This balance is particularly relevant for subsequent exposure analysis, where overestimation could artificially inflate the number of exposed elements.

4.4. EXPOSURE ASSESSMENT OF BUILDINGS AND RESIDENTS

The spatial distribution of buildings and resident population across the 24 municipalities of the study area is presented in Annex 2 for 2011 and in Annex 3 for 2021. The number of buildings was calculated by aggregating the building points by municipal administrative codes, while resident population was derived from census data and redistributed to buildings as described in section 2.4. The results show significant spatial heterogeneity, with municipalities such as Lisboa, Sintra and Cascais concentrating the highest numbers of buildings and residents. This spatial heterogeneity is a key component for understanding the municipal-scale evolution of exposure to landslides within the study area.

The exposure assessment for 2021 was conducted by intersecting the binary susceptibility map (very high and high susceptibility as Class 1 and moderate susceptibility as Class 2) with the spatial datasets representing buildings and resident population. As described in the methodological framework, the susceptibility map was reclassified into two operational classes corresponding to areas that together contain 90% of the mapped landslides (Class 1 and Class 2). The exposure analysis therefore considers only the buildings and residents located within this susceptibility domain.

Within the susceptibility domain (Class 1 and Class 2), a total of 11,655 buildings were identified in 2021. Of these, 2,966 buildings fall within the highest susceptibility class (Class 1), while 8,689 buildings are located in the remaining susceptibility class (Class 2). This means

that 25.45% of the buildings contained within the susceptibility domain are located in the highest susceptibility areas (Table 3).

Table 3: Exposure of buildings inside the most critical susceptibility classes, for both 2011 and 2021

Municipalities	Buildings Class 1 (2011)	Buildings Class 2 (2011)	Buildings Class 1 (2021)	Buildings Class 2 (2021)
Alenquer	488	1101	503	1134
Almada	1	40	1	37
Amadora	6	122	6	114
Arruda dos Vinhos	816	1043	776	1032
Cascais	2	55	1	23
Lisboa	-	46	-	40
Loures	98	873	92	863
Mafra	78	528	96	580
Odivelas	10	479	16	529
Oeiras	-	21	-	23
Palmela	12	76	11	80
Sesimbra	4	129	7	131
Setúbal	29	180	23	177
Sintra	16	701	21	758
Sobral de Monte Agraço	343	783	377	812
Torres Vedras	146	835	157	854
Vila Franca de Xira	873	1495	879	1502

A similar pattern is observed for the resident population. Within the same domain, 32,218 residents were identified in 2021. Among them, 5,631 residents are located in Class 1, while 26,587 residents fall within Class 2. Consequently, 17.48% of the population contained within the susceptibility domain resides in the highest susceptibility areas (Table 4).

Table 4: Exposure of residents inside the most critical susceptibility classes, for both 2011 and 2021

Municipalities	Residents Class 1 (2011)	Residents Class 2 (2011)	Residents Class 1 (2021)	Residents Class 2 (2021)
Alenquer	839	2088	824	2157
Almada	2	95	2	98
Amadora	17	842	16	817
Arruda dos Vinhos	1435	2743	1604	2821
Cascais	5	183	5	67
Lisboa	-	346	-	306
Loures	210	2105	193	2036
Mafra	188	1228	222	1370
Odivelas	38	1844	44	2089
Oeiras	-	93	-	93
Palmela	19	176	19	206
Sesimbra	4	296	6	336
Setúbal	25	380	21	347
Sintra	33	5553	43	5504
Sobral de Monte Agraço	634	1612	663	1661
Torres Vedras	254	1849	268	1956
Vila Franca de Xira	1695	4820	1701	4723

When these values are compared with the total number of buildings and residents in the entire study area, the proportion of exposed elements becomes significantly smaller. The total number of buildings across all municipalities considered in the study is 486,007, while the total resident population amounts to 2,965,852 inhabitants. Within this broader context, the buildings located in Class 1 represent approximately 0.61% of the total building stock, while residents located in Class 1 represent approximately 0.19% of the total population.

The exposure assessment for 2011 was performed using the same methodological framework applied to the 2021 dataset. The binary susceptibility map, representing the areas containing 90% of the mapped landslides, was intersected with the spatial datasets of buildings and resident population corresponding to the year 2011.

Within the susceptibility domain defined by the two susceptibility classes (Class 1 and Class 2), a total of 11,429 buildings were identified in 2011. Among these, 2,922 buildings are located within the highest susceptibility class (Class 1), while 8,507 buildings fall within the remaining susceptibility class (Class 2). Consequently, 25.57% of the buildings contained within the susceptibility domain are located in the highest susceptibility areas.

A similar distribution is observed for the resident population. Within the susceptibility domain, the total population amounts to 31.651 inhabitants. Of these, 5.398 residents are located within Class 1, whereas 26,253 residents fall within Class 2. This means that 17.06% of the population within the susceptibility domain resides in the highest susceptibility areas.

When compared with the total population and building stock of the entire study area, the proportion of exposed elements is relatively small. The total number of buildings across the municipalities considered in the study in 2011 is 474,553, while the total resident population amounts to 2,821,699 inhabitants. So, buildings located in the highest susceptibility class represent approximately 0.62% of the total building stock, while residents located in these areas correspond to approximately 0.19% of the total population.

Overall, the results indicate that, although high-susceptibility areas occupy only a limited portion of the territory, a significant proportion of the buildings and residents located within the susceptibility domain are concentrated in the most unstable sectors.

4.5. TEMPORAL CHANGES IN EXPOSURE (2011-2021)

The temporal evolution of exposure was evaluated by comparing the number of buildings and residents intersecting the susceptibility classes in 2011 and 2021. This comparison was carried out using the same susceptibility thresholds and spatial framework, ensuring methodological consistency between the two datasets.

Within the susceptibility domain (Class 1 + Class 2), the total number of buildings increased from 11,429 in 2011 to 11,655 in 2021, corresponding to a growth of 226 buildings, equivalent to an increase of approximately 1.98%. A similar trend is observed for the resident population,

which increased from 31,651 inhabitants in 2011 to 32,218 inhabitants in 2021, representing a growth of 567 residents (+1.79%).

When focusing specifically on the highest susceptibility areas (Class 1), the number of exposed buildings increased from 2,922 in 2011 to 2,966 in 2021, corresponding to an increase of 44 buildings. The resident population living within these areas also increased slightly, from 5,398 residents to 5,631 residents, representing a growth of 233 inhabitants.

Despite these increases, the relative proportion of exposed elements remains relatively stable. Buildings located in Class 1 represented 25.57% of the buildings within the susceptibility domain in 2011, compared to 25.45% in 2021. Similarly, residents located in Class 1 accounted for 17.06% of the population within the susceptibility domain in 2011, compared to 17.48% in 2021.

When compared to the total building stock and population of the entire study area, the proportion of exposed elements remains limited. Buildings located in the highest susceptibility class represent approximately 0.62% of the total buildings in 2011 and 0.61% in 2021, while residents living in these areas correspond to approximately 0.19% of the total population in both years.

Also, it can be established that the most affected municipalities, in terms of buildings and residents' exposure, are Arruda dos Vinhos, Sobral de Monte Agraço and Vila Franca de Xira, respectively having 39.10%, 27.38% and 18.86% of the total buildings and 31.21%, 22.12% and 23.30% of the total number of residents, exposed in the most susceptible classes in 2011; in 2021, the same municipalities show respectively that 38.60%, 28.11%, and 14.08% of the total buildings and 31.64%, 22.05% and 4.68% of the total number of residents, are exposed in the most susceptible classes (Annex 4).

4.6. EXPOSURE OF THE ROAD NETWORK

The exposure of the road network was evaluated by intersecting the road dataset with the binary susceptibility map (very high and high susceptibility as Class 1 and moderate susceptibility as Class 2) derived from the landslide susceptibility model. The resulting dataset was divided into

two classes corresponding to the susceptibility domain used for the exposure analysis (Class 1 and Class 2).

The spatial distribution of the road network across the study area is shown in Figure 14, where the main road categories (motorway, primary, secondary, tertiary and trunk) are represented according to their functional hierarchy. The overlay between the susceptibility map and the road network allows the identification of road segments located within landslide-prone areas.

Within the susceptibility domain, the road network is divided between the two susceptibility classes (Figure 22).

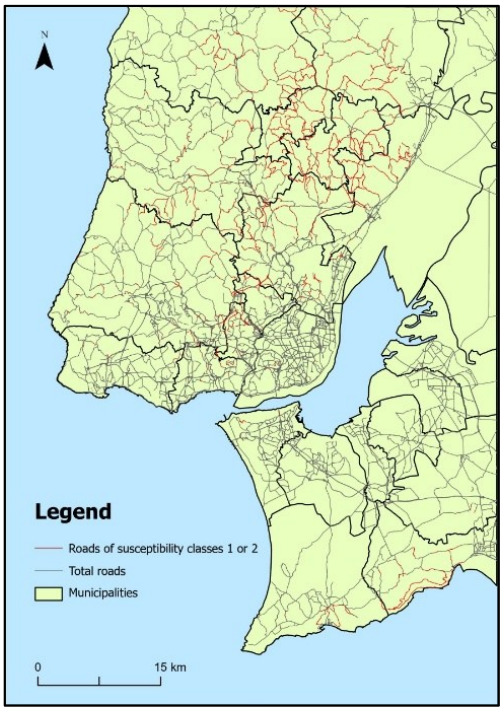

Figure 22: Roads exposed to the most critical susceptibility classes inside of the study area

In Class 1, corresponding to the areas with the highest susceptibility to landslides, a total of 1,223 road segments were identified, corresponding to a cumulative road length of 19,547.58 m. The distribution by road type is as follows:

a) Motorways: 88 segments (3,558.22 m)
b) Primary roads: 329 segments (6,037.44 m)
c) Secondary roads: 144 segments (4,285.14 m)

d) Tertiary roads: 658 segments (5,087.05 m)
e) Trunk roads: 4 segments (579.73 m).

These values indicate that tertiary and primary roads represent the largest proportion of the road network located in the very high susceptible areas.

In Class 2, which represents the moderate susceptibility domain, a significantly larger portion of the road network is present. A total of 4,508 road segments were identified, corresponding to a cumulative length of 35,405.46 m. The distribution by road type is as follows:

a) Motorways: 522 segments (8,848.76 m)
b) Primary roads: 1,173 segments (8,329.03 m)
c) Secondary roads: 598 segments (5,926.17 m)
d) Tertiary roads: 2,196 segments (11,902.86 m)
e) Trunk roads: 19 segments (398.64 m).

As observed for Class 1 and 2, tertiary roads represent the most extensive category in terms of length, reflecting the dense local road network present throughout the municipalities.

When combining both susceptibility classes, the total road network located within the susceptibility domain amounts to 5,731 road segments, with a total length of approximately 54,953 m. Of these, approximately 21.3% of the road segments and 35.6% of the total road length are located within the highest susceptibility class (Class 1).

The spatial relationship between the susceptibility model, the mapped landslide inventory and the road network is illustrated in Figure 23.

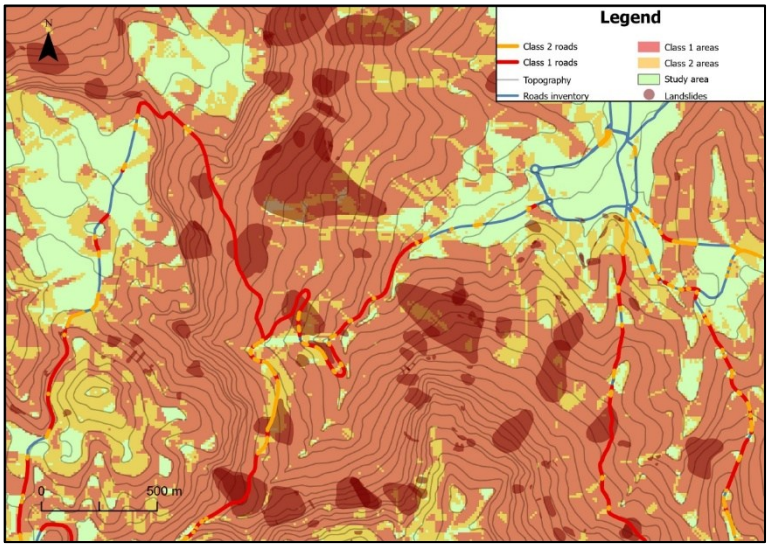

Figure 23: Detail of the susceptibility map with only the two most critical classes (Figure 19), showing the overlap between the landslides, the topography of the area and the roads exposed, with the susceptibility classes.

The map clearly shows that many landslides occur along steep valley slopes and escarpments where roads frequently follow the terrain morphology. This spatial coincidence highlights the interaction between road infrastructure and landslide-prone terrain.

A broader overview of the study area confirms that the road segments classified within susceptibility classes overlap with several sectors where landslides have historically occurred. This spatial correspondence supports the reliability of the susceptibility model and demonstrates its ability to correctly identify terrain sectors where infrastructure may be exposed to landslides.

Overall, the results indicate that the road network, particularly primary and tertiary roads for Class 1, that often follow natural slopes and valley sides and, primary, tertiary roads and motorways for Class 2, represents a relevant exposed element within the study area.

CHAPTER 5: DISCUSSION

The results obtained from the landslide susceptibility modelling and exposure analysis provide important insights into the spatial relationship between landslide-prone terrain and anthropogenic elements in the Lisbon region. The susceptibility model demonstrates a strong predictive performance, as confirmed by the high AUC values obtained during the validation phase (AUC > 0.9), indicating that the selected predisposing factors effectively explain the spatial distribution of the mapped landslides.

The spatial concentration of landslides within a relatively small portion of the study area further confirms the robustness of the model. In particular, the model shows that 90% of the mapped landslides occur within only 16.75% of the study area, highlighting the strong clustering of slope instability processes in specific geomorphological settings.

This concentration is reflected in the distribution of exposed elements. Although the proportion of buildings and population located in the highest susceptibility areas remains relatively small when compared to the total building stock and population of the study area, a significant share of the elements located within the susceptibility domain falls within the highest susceptibility class. This indicates that certain sectors of the territory concentrate both geomorphological susceptibility and human activities, potentially increasing landslide risk at the local scale.

5.1. ROLE OF PREDISPOSING FACTORS IN LANDSLIDE OCCURRENCE

The analysis of the Information Value (IV) scores highlights the relative importance of the predisposing factors controlling landslide occurrence within the study area. As shown in Table 1, slope-related variables consistently exhibit the highest IV values across all training models (AB, AC and BC), confirming that slope gradient represents the dominant geomorphological control on landslide initiation.

In particular, the highest susceptibility is associated with slopes exceeding 45° of steepness, followed by slopes between 40° and 45°, which maintain high and stable IV scores in all model combinations. This pattern reflects the fundamental mechanical role of slope steepness in gravitational instability processes. As slope gradients increase, the shear stress acting on the

soil or rock mass also increases, progressively reducing the stability of the slope and facilitating the occurrence of mass movements. The strong and consistent ranking of slope classes therefore confirms the primary role of terrain morphology in controlling landslide distribution within the Lisbon region.

Lithological and soil properties also play a significant role in landslide susceptibility. Several soil classes, particularly clay-rich vertic soils (Kvcd) and red vertic soils (Vcr), display high IV scores across multiple training models. These results suggest that the mechanical properties of these soil units, such as grain composition, cohesion and permeability, strongly influence slope stability. Materials with lower shear strength or higher susceptibility to water infiltration may promote slope weakening, especially during periods of intense rainfall.

Geological units also exhibit relatively high and stable IV values, confirming the influence of lithology and structural characteristics on landslide occurrence. Certain geological formations appear to be more prone to instability, likely due to differences in rock strength, weathering patterns or structural discontinuities. The presence of layered sedimentary formations and weak lithological contacts may facilitate the development of failure surfaces, contributing to the spatial clustering of landslides observed in the susceptibility map.

Hydrological and morphometric indices such as Topographic Wetness Index (TWI) and Topographic Position Index (TPI) show moderate but consistent contributions to landslide susceptibility. These indices reflect the influence of topographic control on water accumulation and relative landscape position. Areas characterized by higher potential water accumulation can experience increased pore-water pressure during rainfall events, which may reduce effective stress and promote slope failure. Although their IV values are lower than those of slope and certain lithological variables, their stability across the models indicates a consistent secondary influence on landslide predisposition.

Conversely, variables such as aspect and plan curvature display comparatively low IV scores. While concave curvature and certain slope orientations show small positive contributions, their overall influence appears limited. These parameters may locally affect micro-scale processes such as water concentration or differential weathering, but their role in explaining landslide distribution at the regional scale of the study appears less significant.

Therefore, the susceptibility patterns identified in the present work also reflect geomorphological controls that have been widely documented in northern Lisbon. Landslides in this region are predominantly associated with structures where geological and geomorphological conditions favour slope instability processes. As reported in previous studies, landslides north of Lisbon commonly occur in sedimentary formations characterized by alternating permeable and impermeable layers, where water infiltration and groundwater accumulation reduce shear strength and promote slope failure [36]. These mechanisms are compatible with the results obtained in this study, where high IV scores were associated with steep slope classes and specific lithological and soil units.

Overall, the strong agreement in the ranking of predisposing factors across the three training models demonstrates the robustness of the susceptibility analysis. The results indicate that landslide occurrence in the Lisbon region is primarily controlled by a combination of terrain morphology (slope), lithological and soil properties, and hydrological–topographic conditions, with slope gradient representing the most influential factor.

5.2. SPATIAL AND TEMPORAL RELATIONSHIP BETWEEN LANDSLIDES AND EXPOSED ELEMENTS

The exposure analysis highlights a clear spatial relationship between landslide-prone terrain and the distribution of anthropogenic elements within the study area. By intersecting the susceptibility map with datasets representing buildings, resident population and road infrastructure, it is possible to identify the sectors where geomorphological susceptibility and human activities spatially overlap.

Although the proportion of exposed elements remains relatively small when compared to the total number of buildings and residents in the study area, a significant concentration of infrastructure is located within the susceptibility domain. In 2021, a total of 2,966 buildings and 5,631 residents were located within the highest susceptibility class, while 8,689 buildings and 26,587 residents were located in the second susceptibility class. When compared with the total building stock (486,007 buildings) and population (2,965,852 inhabitants), these values

represent only a small fraction of the overall urban system. However, within the susceptibility domain itself, the proportion of exposed elements becomes considerably more significant, indicating that specific sectors of the territory concentrate both unstable terrain and human activities.

A similar spatial relationship is observed for the road network. The intersection between the susceptibility map and the road dataset shows that 1,223 road segments, corresponding to approximately 19.5 km of road length, are located within the highest susceptibility areas. These segments are mainly composed of tertiary and primary roads, which frequently follow valley slopes and hillside alignments due to topographic constraints. As a result, transport infrastructure often intersects sectors where geomorphological conditions favour slope instability.

The spatial distribution of landslides, susceptibility classes and road infrastructure further confirms this relationship. As shown in the susceptibility and road network maps (Figure 23), many landslides occur along slopes where roads run parallel to valley sides or cut through steep terrain. In such contexts, road construction and slope modification may locally alter natural drainage conditions or slope geometry, potentially increasing susceptibility to slope failures. At the same time, roads themselves represent critical exposed elements, as landslides can directly disrupt transport connectivity and accessibility.

Beyond the spatial distribution of exposed elements, the comparison between 2011 and 2021 provides additional insight into the temporal evolution of landslide exposure. Over this ten-year period, the number of buildings within the susceptibility domain increased from 11,429 to 11,655, while the resident population increased from 31,651 to 32,218 inhabitants. Although these increases are relatively moderate, they indicate a gradual expansion of human activities within areas potentially affected by landslide processes.

The changes are particularly noticeable within the highest susceptibility class (Class 1), where the number of buildings increased from 2,922 in 2011 to 2,966 in 2021, and the number of residents increased from 5,398 to 5,631. This trend suggests that, even though landslide-prone areas represent only a limited portion of the territory, urban development and population distribution continue to evolve within these sectors.

The spatial relationship between landslide susceptibility and exposed elements identified in this study is consistent with previous research conducted in the Lisbon region and in comparable geomorphological contexts.

In a study regarding the area north of Lisbon, it is stated that landslides have historically produced damage to property and widespread disruption of roads, highlighting the vulnerability of transport infrastructure located in landslide-prone terrain [36]. Moreover, the same study emphasizes the potential implications for land-use planning, noting that without mitigation measures, construction of buildings and roads in hazardous zones will tend to increase in the near future, and so will landslide risk, illustrating how exposure dynamics may progressively amplify risk conditions.

The relationship between susceptibility patterns and exposed elements observed in this work is also comparable with municipal scale analyses conducted in the Lisbon metropolitan area. Studies focusing on the Loures municipality have shown that a relatively small portion of the population and building stock may be located within the most hazardous sectors, while these areas nevertheless concentrate a large proportion of expected landslide occurrence. For example, it has been reported that only 0.9% of the population and 0.8% of the buildings are located in areas where approximately 75% of future landslides are expected to occur, illustrating the spatial asymmetry between the distribution of susceptible terrain and the concentration of exposed elements [37].

Overall, the comparison with previous studies indicates that the susceptibility and exposure patterns identified in this work are consistent with those previously documented in the Lisbon region. The susceptibility map reflects the main geomorphological controls on landslide occurrence documented in early studies, while the exposure analysis highlights the practical implications of these patterns for buildings, population and infrastructure. The integration of susceptibility modelling with spatial exposure data therefore provides a useful framework for identifying sectors where the interaction between slope instability and human activities may be more critical for territorial planning and landslide risk management.

5.3. IMPLICATIONS OF SUSCEPTIBILITY MODELLING FOR LANDSLIDE RISK MANAGEMENT

The susceptibility model developed in this study provides an effective framework for identifying terrain sectors where landslide occurrence is more likely, offering a valuable tool for supporting landslide risk management and territorial planning. Susceptibility mapping is one of the most widely used approaches for predicting the spatial distribution of landslides, as it allows the identification of areas where geomorphological, geological and hydrological conditions favour slope instability.

The susceptibility map generated in this research highlights a clear spatial pattern in the distribution of landslide-prone terrain. As shown in the susceptibility map with five classes (Figure 21), the highest susceptibility areas are concentrated primarily along steep slopes and geomorphologically dissected sectors of the study area, particularly in the northern and eastern portions of the Lisbon region. In contrast, the western coastal plains and the large low-relief sectors surrounding the Tagus estuary are characterized by lower susceptibility values, reflecting gentler slopes and more stable geomorphological conditions.

The reclassification of the susceptibility map into two main susceptibility domains further emphasizes the concentration of landslide-prone terrain within relatively limited portions of the territory. The binary susceptibility map (Figure 22) highlights how the highest susceptibility classes form discontinuous but clearly identifiable belts associated with steep slopes and valley systems.

The analysis of the cumulative distribution of landslide area shows that a large proportion of the mapped landslides is concentrated within a relatively small fraction of the study area, indicating that the susceptibility model successfully captures the spatial distribution of slope instability processes.

From a risk management perspective, these results provide a valuable basis for identifying priority areas where landslide monitoring, mitigation measures and territorial planning strategies should be concentrated. By highlighting sectors where slope instability processes are more likely to occur, susceptibility modelling allows decision makers to focus preventive actions on areas where the potential impact of landslides may be highest.

The identification of sectors characterized by higher susceptibility also allows planners and decision makers to integrate geomorphological constraints into land-use strategies, particularly in areas where urban expansion and infrastructure development intersect unstable terrain.

The spatial distribution of the susceptibility classes highlights how landslide prone areas frequently coincide with dissected slopes and valley systems where transport infrastructure and local settlements tend to develop. As illustrated in the overlay between landslide inventory, road network and susceptibility classes (Figure 23), several road segments cross terrain characterized by high and very high susceptibility values. This spatial configuration is particularly relevant for risk management, since transport corridors built along slopes or valley flanks are especially vulnerable to slope failures and may experience disruptions during landslide events.

Previous studies conducted in the Lisbon region emphasize the importance of incorporating susceptibility and risk analyses into planning strategies in order to reduce potential damage. In probabilistic landslide risk analyses carried out north of Lisbon, it has been noted that the progressive expansion of settlements and infrastructure into unstable sectors may significantly increase future landslide risk if adequate mitigation measures are not implemented [36]. In particular, the construction of buildings and roads in hazardous zones has been identified as a factor that may lead to a progressive increase in exposure and therefore in the potential consequences of landslide events.

In this context, susceptibility maps represent an essential decision-support tool for territorial management. They can guide the definition of zoning regulations, infrastructure planning and hazard mitigation strategies, helping authorities to identify sectors where urban development should be limited or carefully regulated, as well as areas where engineering stabilization measures or monitoring systems may be required.

Furthermore, the integration of susceptibility modelling with exposure data, as performed in this study, allows a more comprehensive understanding of landslide risk patterns. The identification of buildings, population and road infrastructure located within susceptible sectors highlights how geomorphological hazards interact with human activities across the territory. In particular, the concentration of exposed infrastructure within susceptible areas suggests that even moderate landslide events may produce significant local impacts, especially in sectors where transport connectivity or residential areas depend on slope-side infrastructure.

Overall, the results of this study confirm that susceptibility modelling represents a fundamental component of landslide risk assessment and territorial planning. When combined with detailed information on exposed elements, susceptibility maps can provide a robust basis for supporting preventive strategies aimed at reducing landslide impacts and improving the resilience of human settlements in landslide-prone regions.

Despite the robustness of the susceptibility model developed in this study, several limitations should be acknowledged when interpreting the results and their implications for landslide risk management.

First, the susceptibility analysis focuses exclusively on the spatial probability of landslide occurrence, without explicitly incorporating the temporal probability of landslide events. As a consequence, the model identifies areas where landslides are more likely to occur based on terrain conditions and past landslide distribution, but it does not provide information about the frequency or return period of future landslide events. In this context, susceptibility can be considered a spatial proxy for landslide hazard, particularly when detailed temporal data on landslide recurrence are not available. While this approach is commonly adopted in regional-scale studies, the integration of temporal probability information would further improve the characterization of landslide hazard.

A second limitation concerns the quality and completeness of the landslide inventory used to calibrate the model. Landslide inventories represent a fundamental component of susceptibility modelling, as they define the spatial distribution of past slope failures used to identify the relationships between landslides and predisposing factors. However, inventories are often affected by uncertainties related to mapping resolution, detection methods or the possible underrepresentation of smaller landslide events. Consequently, some slope instability processes may not be fully captured in the dataset, which may influence the statistical relationships identified by the model.

Another important aspect relates to the selection of predisposing factors used in the modelling process. Although the independent variables included in this study, such as slope, elevation, geology, soil type and morphometric indices, represent key factors controlling slope instability, other variables may also influence landslide occurrence. For instance, land use changes, vegetation cover, and anthropogenic slope modifications are known to play an important role

in landslide susceptibility. The absence of these variables in the model may limit the representation of some local instability processes.

Furthermore, the spatial resolution of the input datasets represents an additional constraint. The morphometric variables derived from the DEM were analysed at a resolution of 10 m × 10 m, while geological and soil datasets were available at a 1:25,000 scale. Although these resolutions are appropriate for regional-scale susceptibility analyses, they may not fully capture small-scale geomorphological features or localized instability processes. As a result, the susceptibility map should primarily be interpreted as a regional planning tool rather than as a detailed prediction of individual landslide events.

Despite these limitations, the model demonstrates strong predictive performance, as indicated by the high validation scores obtained during the modelling process. The consistent ranking of conditioning factors across the different training models and the high AUC values confirm the reliability of the statistical relationships identified between landslide occurrence and terrain characteristics. This suggests that the susceptibility model provides a robust representation of the spatial patterns of landslide occurrence within the study area.

Future research could further support a more comprehensive assessment of landslide risk in the Lisbon region by integrating additional datasets and modelling approaches. In particular, the incorporation of rainfall thresholds, antecedent rainfall conditions and land use dynamics could provide valuable insights into landslide triggering and changes in exposure over time. Similarly, the integration of susceptibility modelling with quantitative vulnerability assessments and economic loss estimation would allow a more comprehensive evaluation of landslide risk and its potential socio-economic impacts.

Overall, while the susceptibility model developed in this study provides an effective tool for identifying landslide-prone areas, its results should be interpreted together with detailed exposure and vulnerability information in order to support effective landslide risk management and territorial planning strategies.

CHAPTER 6: CONCLUSIONS

6.1. KEY FINDINGS

This study demonstrates that landslide susceptibility in the Lisbon region is strongly controlled by a combination of topographic, geological and pedological factors, with slope gradient emerging as the dominant predisposing variable. Steep slopes (>40°) show the highest susceptibility, confirming the primary role of terrain morphology in slope instability processes. The susceptibility model shows high predictive performance (AUC > 0.9), indicating that the selected conditioning factors effectively capture the spatial distribution of landslides. In addition to slope, specific lithological and soil units significantly contribute to susceptibility, highlighting the importance of material properties and hydrological conditions in controlling slope failure.

Despite the limited spatial extent of highly susceptible areas, the results reveal a clear concentration of exposed elements within these sectors. This indicates that landslide risk is spatially localized but potentially significant where susceptible terrain and human activities overlap.

6.2. EXPOSURE AND TEMPORAL EVOLUTION

The exposure analysis shows that only a small proportion of the total building stock and population is located within the highest susceptibility areas. However, within the susceptibility domain, a substantial share of buildings and residents is concentrated in the most unstable sectors.

The comparison between 2011 and 2021 highlights a moderate increase in both buildings and population within susceptible areas. Although this growth is limited, it suggests a gradual expansion of human activities into landslide-prone terrain, which may contribute to a progressive increase in potential risk over time.

The analysis of the road network further confirms the interaction between infrastructure and unstable slopes, particularly where transport corridors follow valley sides and steep terrain.

6.3. IMPLICATIONS FOR RISK MANAGEMENT

The results confirm that landslide susceptibility mapping represents an effective tool for supporting land-use planning and risk management. The identification of spatially concentrated susceptible areas allows decision-makers to prioritize monitoring, mitigation measures and planning restrictions.

The integration of susceptibility and exposure provides a more comprehensive framework for identifying critical areas where landslide impacts may be more severe. This approach is particularly relevant in regions undergoing urban development, where even moderate increases in exposure can influence future risk patterns.

6.4. LIMITATIONS AND FUTURE PERSPECTIVES

This study is based on a susceptibility approach and does not explicitly account for the temporal probability of landslide occurrence. As a result, the analysis provides a spatial representation of potential instability but does not quantify event frequency.

Additional limitations include the absence of dynamic triggering factors such as rainfall intensity and land-use changes, as well as uncertainties related to the completeness of the landslide inventory and the spatial resolution of input data.

Future research should integrate temporal hazard modelling, rainfall thresholds and land-use dynamics, as well as quantitative vulnerability assessments, in order to provide a more comprehensive evaluation of landslide risk.

REFERENCES

1. Cruden D. Cruden,D.M.,Varnes, D.J.,1996, Landslide Types and Processes, Transportation Research Board, U.S. National Academy of Sciences, Special Report, 247: 36-75. *Special Report - National Research Council, Transportation Research Board*. 1996;247:36-57.

2. Carvalho J, Dias R, Borges J, Quental L, Caldeira B. Soil Classification Maps for the Lower Tagus Valley Area, Portugal, Using Seismic, Geological, and Remote Sensing Data. *Remote Sensing*. 2025;17(8). doi:10.3390/rs17081376

3. Kullberg J, Rocha R, Soares AF, et al. A Bacia Lusitaniana: Estratigrafia, Paleogeografia e Tectónica. *Geologia de Portugal No Contexto da Ibéria*. Published online January 1, 2006:317-368.

4. Crozier MJ, Glade T. Landslide Hazard and Risk: Issues, Concepts and Approach. In: *Landslide Hazard and Risk*. John Wiley & Sons, Ltd; 2005:1-40. doi:10.1002/9780470012659.ch1

5. Fell R. Landslide risk assessment and acceptable risk. *Can Geotech J*. 1994;31(2):261-272. doi:10.1139/t94-031

6. Cruden D, Fell R. *Landslide Risk Assessment*. Routledge; 2018.

7. Uzielli M, Nadim F, Lacasse S, Kaynia AM. A conceptual framework for quantitative estimation of physical vulnerability to landslides. *Engineering Geology*. 2008;102(3):251-256. doi:10.1016/j.enggeo.2008.03.011

8. Brabb E.E. Innovative approaches to landslide hazard and risk mapping. *in Proceedings of IVth International Conference and Field Workshop in Landslides*. Published online August 23, 1984:17-22.

9. Statistics Portugal - Press Release 707257820. Accessed February 8, 2026. https://www.ine.pt/xportal/xmain?xpid=INE&xpgid=ine_destaques&DESTAQUESdest_boui=707257820&DESTAQUEStema=5414321&DESTAQUESmodo=2

10. Cuervas-Mons J, Zêzere JL, Domínguez-Cuesta MJ, et al. Assessment of Urban Subsidence in the Lisbon Metropolitan Area (Central-West of Portugal) Applying Sentinel-1 SAR Dataset and Active Deformation Areas Procedure. *Remote Sensing*. 2022;14(16). doi:10.3390/rs14164084

11. Oliveira, L., Gomes, R. C., Amoroso, S., Pagliaroli, A., & Teves-Costa, P. (2024). Seismic site effects in Lisbon: the role of complex geological and morphological conditions. Bulletin of Earthquake Engineering, 22(10), 4915-4958.

12. Zêzere JL, de Brum Ferreira A, Rodrigues ML. The role of conditioning and triggering factors in the occurrence of landslides: a case study in the area north of Lisbon (Portugal). *Geomorphology*. 1999;30(1):133-146. doi:10.1016/S0169-555X(99)00050-1

13. Zêzere JL, Trigo RM, Trigo IF. Shallow and deep landslides induced by rainfall in the Lisbon region (Portugal): assessment of relationships with the North Atlantic Oscillation. *Natural Hazards and Earth System Sciences*. 2005;5(3):331-344. doi:10.5194/nhess-5-331-2005

14. Zêzere JL, Reis E, Garcia R, et al. Integration of spatial and temporal data for the definition of different landslide hazard scenarios in the area north of Lisbon (Portugal). *Natural Hazards and Earth System Sciences*. 2004;4(1):133-146. doi:10.5194/nhess-4-133-2004

15. Zêzere JL, Oliveira SC, Garcia RAC, Reis E. Landslide risk analysis in the area North of Lisbon (Portugal): evaluation of direct and indirect costs resulting from a motorway disruption by slope movements. *Landslides*. 2007;4(2):123-136. doi:10.1007/s10346-006-0070-z

16. Landslide risk analysis in the area North of Lisbon (Portugal): evaluation of direct and indirect costs resulting from a motorway disruption by slope movements | Landslides | Springer Nature Link. Accessed February 8, 2026. https://link.springer.com/article/10.1007/s10346-006-0070-z

17. van Westen CJ, Castellanos E, Kuriakose SL. Spatial data for landslide susceptibility, hazard, and vulnerability assessment: An overview. *Engineering Geology*. 2008;102(3):112-131. doi:10.1016/j.enggeo.2008.03.010

18. Corominas J, van Westen C, Frattini P, et al. Recommendations for the quantitative analysis of landslide risk. *Bull Eng Geol Environ*. 2014;73(2):209-263. doi:10.1007/s10064-013-0538-8

19. Zêzere JL, Garcia RAC, Oliveira SC, Reis E. Probabilistic landslide risk analysis considering direct costs in the area north of Lisbon (Portugal). *Geomorphology*. 2008;94(3):467-495. doi:10.1016/j.geomorph.2006.10.040

20. BEVEN KJ, KIRKBY MJ. A physically based, variable contributing area model of basin hydrology / Un modèle à base physique de zone d'appel variable de l'hydrologie du

bassin versant. *Hydrological Sciences Bulletin*. 1979;24(1):43-69. doi:10.1080/02626667909491834

21. Garcia RAC, Oliveira SC, Zêzere JL. Assessing population exposure for landslide risk analysis using dasymetric cartography. *Natural Hazards and Earth System Sciences*. 2016;16(12):2769-2782. doi:10.5194/nhess-16-2769-2016

22. Melo R, Zêzere JL, Oliveira SC, et al. Defining evacuation travel times and safety areas in a debris flow hazard scenario. *Science of The Total Environment*. 2020;712:136452. doi:10.1016/j.scitotenv.2019.136452

23. Soeters R, Westen CJ van. Slope instability recognition, analysis, and zonation. In: *Landslides, Investigation and Mitigation*. National Academy Press; 1996:129-177. Accessed March 20, 2026. https://research.utwente.nl/en/publications/slope-instability-recognition-analysis-and-zonation/

24. Carrara A, Guzzetti F, Cardinali M, Reichenbach P. Use of GIS Technology in the Prediction and Monitoring of Landslide Hazard. *Natural Hazards*. 1999;20(2):117-135. doi:10.1023/A:1008097111310

25. Guzzetti F, Carrara A, Cardinali M, Reichenbach P. Landslide hazard evaluation: a review of current techniques and their application in a multi-scale study, Central Italy. *Geomorphology*. 1999;31(1):181-216. doi:10.1016/S0169-555X(99)00078-1

26. Aleotti P, Chowdhury R. Landslide hazard assessment: summary review and new perspectives. *Bull Eng Geol Env*. 1999;58(1):21-44. doi:10.1007/s100640050066

27. Dai FC, Lee CF, Ngai YY. Landslide risk assessment and management: an overview. *Engineering Geology*. 2002;64(1):65-87. doi:10.1016/S0013-7952(01)00093-X

28. Chacón J, Irigaray C, Fernández T, El Hamdouni R. Engineering geology maps: landslides and geographical information systems. *Bull Eng Geol Environ*. 2006;65(4):341-411. doi:10.1007/s10064-006-0064-z

29. Fell R, Corominas J, Bonnard C, Cascini L, Leroi E, Savage WZ. Guidelines for landslide susceptibility, hazard and risk zoning for land use planning. *Engineering Geology*. 2008;102(3):85-98. doi:10.1016/j.enggeo.2008.03.022

30. L YK. Statistical prediction model for slope instability of metamorphosed rocks. *Proceedings of the 5th International Symposium on Landslides*. 1988;2:1269-1272.

31. Guzzetti F. *Landslide Hazard and Risk Assessment*. Thesis. Universitäts- und Landesbibliothek Bonn; 2006. Accessed February 19, 2026. https://bonndoc.ulb.uni-bonn.de/xmlui/handle/20.500.11811/2644

32. Gorsevski P, Gessler PE, Foltz RB. *Spatial Prediction of Landslides Hazard Using Logistic Regression and GIS*. 2000:8.

33. Oliveira SC, Zêzere JL, Catalão J, Nico G. The contribution of PSInSAR interferometry to landslide hazard in weak rock-dominated areas. *Landslides*. 2015;12(4):703-719. doi:10.1007/s10346-014-0522-9

34. Pereira S, Garcia RAC, Zêzere JL, Oliveira SC, Silva M. Landslide quantitative risk analysis of buildings at the municipal scale based on a rainfall triggering scenario. *Geomatics, Natural Hazards and Risk*. 2017;8(2):624-648. doi:10.1080/19475705.2016.1250116

35. Zêzere JL, Pereira S, Melo R, Oliveira SC, Garcia RAC. Mapping landslide susceptibility using data-driven methods. *Science of The Total Environment*. 2017;589:250-267. doi:10.1016/j.scitotenv.2017.02.188

36. Zêzere JL, Garcia RAC, Oliveira SC, Reis E. Probabilistic landslide risk analysis considering direct costs in the area north of Lisbon (Portugal). *Geomorphology*. 2008;94(3):467-495. doi:10.1016/j.geomorph.2006.10.040

37. Guillard-Gonçalves C, Zêzere JL. Combining Social Vulnerability and Physical Vulnerability to Analyse Landslide Risk at the Municipal Scale. *Geosciences*. 2018;8(8). doi:10.3390/geosciences8080294

ANNEXES

Annex 1: Total length of road (km) per municipality and for each road type.

Municipality	Total Length	Motorway	Trunk	Primary	Secondary	Tertiary
Alcochete	**122.16**	32.63	10.41	31.87	44.01	7.43
Alenquer	**230.89**	35.71	28.38	59.65	96.05	0.00
Almada	**208.93**	29.05	22.32	46.45	57.54	21.57
Amadora	**162.88**	19.47	18.85	38.16	47.12	28.20
Arruda dos Vinhos	**140.88**	14.78	13.06	30.63	51.23	0.00
Azambuja	**61.02**	24.77	12.63	23.19	25.57	0.00
Barreiro	**111.17**	21.51	12.07	20.42	28.51	17.32
Benavente	**41.73**	13.81	5.45	8.61	13.83	0.66
Cascais	**261.61**	32.99	27.16	42.49	62.45	2.28
Lisboa	**543.37**	30.12	34.28	57.34	97.86	108.62
Loures	**469.22**	94.61	41.88	91.66	124.83	34.29
Mafra	**455.21**	68.10	34.42	76.20	120.59	5.10
Moita	**113.76**	20.24	9.65	18.64	24.94	12.20
Montijo	**131.16**	26.63	13.95	24.66	34.27	8.13
Odivelas	**103.89**	13.64	10.45	18.42	24.03	22.14
Oeiras	**206.83**	34.31	25.73	36.56	48.91	17.11
Palmela	**198.79**	47.40	24.81	53.45	74.69	1.82
Seixal	**204.48**	61.47	20.48	46.58	62.80	1.93
Sesimbra	**164.2**	7.50	6.35	16.08	33.52	0.00
Setúbal	**186.41**	13.71	10.98	21.87	33.35	0.56
Sintra	**552.45**	53.04	37.66	72.54	126.03	36.38

Sobral de Monte Agraço	**120.3**	16.61	6.74	17.21	31.62	0.00
Torres Vedras	**280.8**	33.97	19.52	46.83	75.32	0.00
Vila Franca de Xira	**262.64**	86.59	31.47	64.88	96.10	2.39

Annex 2: Number of buildings and residents per municipality (2011)

Municipality	District	Number of Buildings (2011)	Total Residents (2011)
Alcochete	**Setúbal**	4,567	17,515
Alenquer	**Lisboa**	13,070	37,577
Almada	**Setúbal**	34,343	173,409
Amadora	**Lisboa**	13,719	175,075
Arruda dos Vinhos	**Lisboa**	4,754	13,387
Azambuja	**Lisboa**	2,456	7,235
Barreiro	**Setúbal**	11,024	78,735
Benavente	**Santarém**	2,601	9,127
Cascais	**Lisboa**	43,650	206,439
Lisboa	**Lisboa**	52,546	548,358
Loures	**Lisboa**	31,144	204,898
Mafra	**Lisboa**	28,008	76,676
Moita	**Setúbal**	12,408	66,013
Montijo	**Setúbal**	10,139	45,551
Odivelas	**Lisboa**	16,371	144,488
Oeiras	**Lisboa**	18,247	172,130
Palmela	**Setúbal**	16,070	51,055

Seixal	**Setúbal**	30,145	158,239
Sesimbra	**Setúbal**	20,436	49,496
Setúbal	**Setúbal**	18,156	96,856
Sintra	**Lisboa**	56,917	377,823
Sobral de Monte Agraço	**Lisboa**	4,113	10,156
Torres Vedras	**Lisboa**	21,728	57,249
Vila Franca de Xira	**Lisboa**	12,559	27,965

Annex 3: number of buildings and residents per municipality (2021)

Municipality	**District**	**Number of Buildings (2021)**	**Total Residents (2021)**
Alenquer	**Lisboa**	13,056	39,038
Arruda dos Vinhos	**Lisboa**	4,684	13,985
Azambuja	**Lisboa**	2,436	7,100
Cascais	**Lisboa**	44,226	214,093
Lisboa	**Lisboa**	49,223	545,627
Loures	**Lisboa**	31,353	201,249
Mafra	**Lisboa**	28,790	86,485
Oeiras	**Lisboa**	18,488	17,1650
Sintra	**Lisboa**	57,759	385,557
Sobral de Monte Agraço	**Lisboa**	4,230	10,538
Torres Vedras	**Lisboa**	21,933	58,952
Vila Franca de Xira	**Lisboa**	16,914	137,404
Amadora	**Lisboa**	12,542	171,440
Odivelas	**Lisboa**	16,974	148,000
Benavente	**Santarém**	2,645	9,531

Alcochete	**Setúbal**	4,595	19,074
Almada	**Setúbal**	34,518	176,929
Barreiro	**Setúbal**	10,871	78,325
Moita	**Setúbal**	12,232	66,234
Montijo	**Setúbal**	10,117	49,980
Palmela	**Setúbal**	16,460	56,629
Seixal	**Setúbal**	32,204	166,486
Sesimbra	**Setúbal**	21,593	52,378
Setúbal	**Setúbal**	18,164	99,168

Annex 4: % of exposed elements to the total buildings and residents' inventory.

Municipality	District	Percentage of exposure of Buildings (2011)	Percentage of exposure of Residents (2011)	Percentage of exposure of Buildings (2021)	Percentage of exposure of Residents (2021)
Alenquer	**Lisboa**	12.16%	7.79%	12.54%	7.64%
Almada	**Setúbal**	0.12%	0.06%	0.11%	0.06%
Amadora	**Lisboa**	0.93%	0.49%	0.96%	0.49%
Arruda dos Vinhos	**Lisboa**	39.10%	31.21%	38.60%	31.64%
Cascais	**Lisboa**	0.13%	0.09%	0.05%	0.03%
Lisboa	**Lisboa**	0.09%	0.06%	0.08%	0.06%
Loures	**Lisboa**	3.12%	1.13%	3.05%	1.11%
Mafra	**Lisboa**	2.16%	1.84%	2.35%	1.84%
Odivelas	**Lisboa**	2.99%	1.30%	3.21%	1.44%
Oeiras	**Lisboa**	0.12%	0.05%	0.12%	0.05%
Palmela	**Setúbal**	0.55%	0.38%	0.55%	0.40%
Sesimbra	**Setúbal**	0.66%	0.61%	0.64%	0.66%
Setúbal	**Setúbal**	1.16%	0.42%	1.10%	0.37%
Sintra	**Lisboa**	1.26%	1.48%	1.35%	1.44%
Sobral de Monte Agraço	**Lisboa**	27.38%	22.12%	28.11%	22.05%
Torres Vedras	**Lisboa**	4.51%	3.67%	4.61%	3.77%

Vila Franca de Xira	**Lisboa**	18.86%	23.30%	14.08%	4.68%

Annex 5: legend of lithologies corresponding to the geological codes.

Code	Lithology	Code	Lithology	Code	Lithology
(beta)1	Lisbon Volcanic Complex	**J3at**	Claystones and sandstones	**vulcindif**	Undifferentiated volcanic rocks
(beta)1p	Lisbon Volcanic Complex: pyroclastic rocks	**J3Cm**	Conglomerates	**C1LA**	Mudstones and sandstones
(gam)MC	Gabbro-diorite	**J3CR**	Arkoses	**J3Bo**	Sandstones, claystones and conglomerates
(gama)ap	Aplite, microgranite, micropegmatite	**J3Es**	Limestones, sandstones and marls	**J3CM**	Limestones and marls
(gama)S	Granite	**J3FP**	Limestones and marls	**propilit**	Propylitized volcanic rocks
(miu)	Mafic intrusive rocks	**J3Fr**	Sandstones, marls and limestones	**C1-2Al**	Mudstones, sandstones and conglomerates
(phi)Bf	Conglomerates, sandstones and claystones	**J3MG**	Limestone	**C1SS**	Mudstones and sandstone

(phi)Bf_a	Calcareous intercalations	**J3MM**	Limestones and marls	**brectraquit**	Trachytic breccia
(psi)	Quartz-tourmalinite	**J3Q**	Reef limestones	**J3Ot**	Limestones
(sigma)S	Syenite	**J3Ra**	Limestones and marls	**MAc**	Sandstones and claystones
basalt	Basalt dykes and intrusions	**J3So**	Mudstones, sandstones, marls and limestones	**MAc_l**	Sandstones with calcareous intercalations
brecbasalt	Basaltic breccia	**J3SP**	Limestones and marls	**PU**	Sands and sandstones
brecgran	Granitic breccia	**MBP**	Sandstones	**?**	Unknown lithology
brecmaf	Mafic breccia	**MCR**	Sandstones	**MEc**	Limestones
brecsienit_l	Syenitic breccia	**MCV**	Limestones	**PSM**	Sands
brecvulc	Volcanic breccia	**MEs**	Sandstones	**QMF**	Claystones and conglomerates
C1CG	Reef limestones and limestones with Choffatella	**MFF**	Calcarenites and marls	**MPi**	Sandstones and calcarenites
C1Cr	Limestones and marls	**MFT**	Clays	**MQA**	Sands and marls

C1Cx	Limestones and mudstones	**Mgg**	Limestones and clays	**MQT**	Sandstones
C1HB	Heterolithic beds	**MGR**	Sandstones	**MAz**	Claystones and marls
C1LS	Mudstones and sandstones	**Mhm**	Lacustrine limestones	**aluv**	Alluvial deposits
C1Re	Sandstones, mudstones and dolomites	**MMa**	Sandstones	**MPa**	Marly limestones
C1RR	Limestones, sandstones and mudstones	**MMu**	Limestones	**Pag**	Water body
C1SC	Marls, sandstones, limestones and mudstones	**MMv**	Limestones	**C1Ro**	Mudstones, sandstones and conglomerates
C1Se	Mudstones, sandstones and conglomerates	**MPe**	Glauconitic deposits	**J1Da**	Mudstones, dolomitic limestones and evaporites
C1SG	Limestones, marls and sandstones	**Mpm**	Sandstones	**J3Cm**	Conglomerates

C1SL	Mudstones and sandstones	**MPr**	Claystones and limestones	**J3VR**	Clays, sandstones, conglomerates and limestones
C1VG	Volcanic conglomerate	**MQC**	Limestones	**J12CL**	Dolomites
C1VL	Sandstones, conglomerates and mudstones	**MRL**	Deposits	**MGM**	Conglomerates
C2Bi	Bioclastic limestone	**MVC**	Sandstones	**J2Pe**	Limestones
C2Cn	Limestones and sandstones	**MVQ**	Sandstones and limestones	**(phi)Pi**	Conglomerates, sandstones and marls
C2Fa	Conglomerates	**MXa**	Clays	**depvert**	Slope deposits
C2Ga	Limestones and marls	**PSi**	Sandstones	**(phi)SN**	Limestones
dolerit	Dolerite dykes and intrusions	**QBe**	Conglomerates	**J3Az**	Limestones and dolomites
gabr	Gabbro-diorite dykes and intrusions	**Qd**	Consolidated dunes	**ap**	Beach sands
J12G	Marls, limestones and dolomites	**Qi**	Sands and gravels	**C1PC**	Sandstones, mudstones, limestones and dolomites

J1Da	Mudstones, dolomitic limestones and evaporites	**Qm**	Marine deposits	**C1Ma**	Marls and limestones
J1Da_l	Platy dolomites	**QPC**	Sands and claystones	**PSA**	Sandstones and conglomerates
J1MV	Dolomitic marls and dolomitic limestones	**ra_ni**	Undifferentiated igneous rocks	**Qf**	Fluvial terrace deposits
J1VS	Volcano-sedimentary complex	**riolit**	Rhyolite	**Qae**	Aeolian deposits
J3Ab	Marls and mudstones	**techenit**	Techenite	**C1FG**	Sandstones, conglomerates and mudstones
J3Am	Limestones	**traquibasalt**	Trachybasalt		
J3Ar	Limestones and marls	**traquit**	Trachyte		

Annex 6: legend of soil types corresponding to the soil codes.

Code	Soil	Code	Soil	Code	Soil
Nv_asoc	Lithosols / shallow stony soils association	**Lvt**	Vertic leptosols	**Sblc**	Calcareous loamy brown soils
A	Alluvial soils	**Mnlt**	Saline soils	**Scb**	Clay brown soils
Aa	Recent alluvial soils	**Mnst**	Saline hydromorphic soils	**Skb**	Skeletic brown soils
Aac	Calcareous alluvial soils	**Mnstb**	Saline hydromorphic clay soils	**Slb**	Loamy brown soils
Ac	Colluvial soils	**Mnt**	Saline soils	**Sp**	Podzolic brown soils
Al	Fluvisols	**Mnto**	Organic saline soils	**Spc**	Calcareous podzolic brown soils
Alc	Calcareous fluvisols	**Mstb**	Hydromorphic saline soils	**Spcs**	Sandy podzolic soils
Ap	Alluvial plains soils	**Mt**	Hydromorphic soils	**Srt**	Red soils
Aph	Hydromorphic alluvial soils	**Pa**	Arenosols	**Srth**	Hydromorphic red soils
Apr	Recent alluvial soils	**Pab**	Brown arenosols	**Svc**	Vertic soils
Arb	Sandy alluvial soils	**Pac**	Calcareous arenosols	**Va**	Vertisols

Arc	Clayey alluvial soils	**Paco**	Organic calcareous arenosols	**Vac**	Calcareous vertisols
Arct	Clayey terrace alluvial soils	**Pag**	Coastal sandy soils	**Vaco**	Organic calcareous vertisols
Ard	Alluvial soils with drainage limitations	**Pagc**	Calcareous coastal sands	**Vag**	Gley vertisols
Art	Terrace alluvial soils	**Pago**	Organic coastal sands	**Vago**	Organic gley vertisols
As	Sandy soils	**Pao**	Organic arenosols	**Val**	Loamy vertisols
Asa	Sandy alluvial soils	**Par**	Red sandy soils	**Vao**	Organic vertisols
Asac	Calcareous sandy soils	**Pat**	Terrace sandy soils	**Vat**	Terrace vertisols
Asc	Sandy colluvial soils	**Patc**	Calcareous terrace sands	**Vatc**	Calcareous terrace vertisols
Assa	Sandy soil association	**Pato**	Organic terrace sands	**Vato**	Organic terrace vertisols
Assac	Calcareous sandy soil association	**Pc**	Podzols	**Vc**	Vertic cambisols
Assc	Sandy colluvial association	**Pca**	Calcareous podzols	**Vcc**	Calcareous vertic cambisols

At	Terrace soils	**Pcb**	Brown podzols	**Vcd**	Clay vertic soils
Ata	Sandy terrace soils	**Pcd**	Clay podzols	**Vcd#**	Clay vertic soils
Atac	Calcareous terrace soils	**Pcdc**	Calcareous clay podzols	**Vcdc**	Calcareous clay vertic soils
Atc	Clayey terrace soils	**Pcds**	Silty clay podzols	**Vcdt**	Terrace clay vertic soils
Atl	Loamy terrace soils	**Pcr**	Red podzols	**Vcm**	Vertic cambisols
Ba	Cambisols	**Pcs**	Sandy podzols	**Vcmo**	Organic vertic cambisols
Bac	Calcareous cambisols	**Pcsd**	Sandy silty podzols	**Vcsd**	Silty vertic soils
Bc	Clay cambisols	**Pcst**	Sandy terrace podzols	**Vcst**	Sandy vertic soils
Bca	Calcareous clay cambisols	**Pct**	Terrace podzols	**Vct**	Terrace vertic soils
Bp	Podzolic soils	**Pctc**	Calcareous terrace podzols	**Vdc**	Vertic clay soils
Bpac	Calcareous podzolic soils	**Pcz**	Podzols	**Vdg**	Gley vertic soils
Bpca	Clay podzolic soils	**Pdc**	Clay podzols	**Vl**	Vertic luvisols

Bva	Vertic cambisols	**Pdg**	Gley podzols	**Vm**	Vertic Mediterranean soils
Bvac	Calcareous vertic cambisols	**Pgm**	Hydromorphic podzols	**Vmcd**	Clay vertic Mediterranean soils
Bvca	Clay vertic cambisols	**Pl**	Lithosols	**Vt**	Vertic terrace soils
Ca	Calcareous soils	**Pm**	Mediterranean soils	**Vtc**	Calcareous vertic terrace soils
Caa	Calcareous alluvial soils	**Pmcd**	Clay Mediterranean soils	**Vtco**	Organic vertic terrace soils
Caac	Calcareous clay soils	**Pmg**	Gley Mediterranean soils	**Vtdc**	Clay vertic terrace soils
Cac	Calcareous colluvial soils	**Pmn**	Neutral Mediterranean soils	**Vto**	Organic vertic terrace soils
Cal	Calcareous loamy soils	**Pp**	Podzolic soils	**Arg**	Clay soils
Cb	Brown soils	**Ppr**	Red podzolic soils	**Aslc**	Calcareous sandy soils
Cbc	Calcareous brown soils	**Ppt**	Terrace podzolic soils	**Bpc**	Calcareous podzols
Cp	Podzols	**Pt**	Terrace soils	**Calc**	Calcareous soils

Cpc	Calcareous podzols	**Ptc**	Calcareous terrace soils	**Cd**	Clay soils
Cpv	Vertic podzols	**Ptco**	Organic terrace soils	**Mns**	Saline soils
Cpvc	Calcareous vertic podzols	**Pto**	Organic terrace soils	**Pcx**	Podzolic soils
Eb	Eutric cambisols	**Pvd**	Vertic podzols	**Pg**	Gley soils
Ec	Cambisols	**Pz**	Podzols	**Pgn**	Neutral gley soils
Et	Terra rossa soils	**Pzh**	Hydromorphic podzols	**Pmc**	Mediterranean clay soils
Ka	Luvisols	**Qb**	Beach sands	**Ppn**	Neutral podzolic soils
Kac	Calcareous luvisols	**Qta**	Coastal terrace sands	**Ps**	Sandy soils
Kb	Brown luvisols	**Rcg**	Regosols	**Psn**	Neutral sandy soils
Kla	Clay luvisols	**Rg**	Regosols	**Sag**	Sandy alluvial soils
Klb	Brown clay luvisols	**Rgc**	Calcareous regosols	**Sg**	Gley soils
Kr	Red soils	**Sb**	Brown soils	**Sr**	Red soils
Krc	Calcareous red soils	**Sba**	Brown alluvial soils	**Vcdl**	Loamy vertic soils
Kvcd	Clay-rich vertic soils	**Sbac**	Calcareous brown alluvial soils	**Vcr**	Red vertic soils

Lb	Leptosols	**Sbc**	Calcareous brown soils	**Vcs**	Silty vertic soils
Lpt	Lithic leptosols	**Sbl**	Loamy brown soils	**Vtd**	Terrace vertic soils

DICHIARAZIONE SULL'USO DI STRUMENTI DI AI Lo studente dichiara di aver utilizzato strumenti di intelligenza artificiale esclusivamente come supporto alla redazione del testo, nel rispetto delle indicazioni del Consiglio di Corso di Laurea. ***I contenuti scientifici e l'elaborazione critica restano di esclusiva responsabilità dell'autore.***